Master's Theses   Master's Theses and Graduate Research

Fall 2021

A Chemical and Minerological Fingerprint of Hydraulic Mining Sediment, in the Yolo Bypass, California

Stephanie Annette Meursing
San Jose State University

Follow this and additional works at: https://scholarworks.sjsu.edu/etd_theses

A CHEMICAL AND MINEROLOGICAL FINGERPRINT OF HYDRAULIC MINING SEDIMENT,
IN THE YOLO BYPASS, CALIFORNIA

A Thesis

Presented to

The Faculty of the Department of Geology

San José State University

In Partial Fulfillment

of the Requirements for the Degree

Master of Science

by

Stephanie Annette Meursing

December 2021

The Designated Thesis Committee Approves the Thesis Titled

A CHEMICAL AND MINEROLOGICAL FINGERPRINT OF HYDRAULIC MINING SEDIMENT,
IN THE YOLO BYPASS, CALIFORNIA

by

Stephanie Annette Meursing

APPROVED FOR THE DEPARTMENT OF GEOLOGY

SAN JOSÉ STATE UNIVERSITY

December 2021

Emmanuel Gabet, Ph.D.	Department of Geology
Kim Blisniuk, Ph.D.	Department of Geology
Ryan Portner, Ph.D.	Department of Geology

ABSTRACT

A CHEMICAL AND MINEROLOGICAL FINGERPRINT OF HYDRAULIC MINING SEDIMENT,
IN THE YOLO BYPASS, CALIFORNIA

by Stephanie Annette Meursing

Hydraulic gold mining in California, began not long after the discovery of gold in 1848.
This type of mining dislodged large amounts of sediment, which were then deposited
downstream. The Yolo Bypass, downstream from several northern California rivers, has
received and continues to receive hydraulic mining sediment (HMS). The main goal of this
study was to document the chemical and mineralogical characteristics of HMS in the bypass.
Twelve borehole cores from the bypass and five *in-situ* auriferous gravel samples, which
were used for background concentrations, were collected for this study. All twelve cores
had higher Hg concentrations than the *in-situ* auriferous gravels. The Hg concentrations in
the bypass range from 0.034 ppm to 1.32 ppm. Background concentrations from the five *in-situ* auriferous gravel samples range from 0.010 ppm to 0.098 ppm. Using specific chemical
and mineralogical indices such as Hg, Al/Ca, CaO, Ca/Sr, Ni/Zr, and quartz/plagioclase,
fractions of sediment containing HMS were estimated. The fractions of sediment containing
HMS, in the eastern bypass cores, range from 73% to 94%. Hydrologic banding, visually
distinct threads of flow, with little lateral mixing due to shallow depths, occurs in the
bypass. This study has identified distinct chemical and mineralogical differences between
each band, primarily when considering Hg concentrations.

ACKNOWLEDGMENTS

TABLE OF CONTENTS

LIST OF TABLES

LIST OF FIGURES

INTRODUCTION

Tertiary Gravels

Throughout the Eocene-Oligocene, fluvial sediments and gravels were deposited in the Sierra Nevada valleys (Cassel and Graham, 2011). These gravels, known for their high concentrations of placer gold, are identified by many names including Tertiary gravels, auriferous gravels, pre-volcanic gravels, and Eocene-Oligocene gravels (Lindgren, 1911; Cassel and Graham, 2011). These auriferous gravel deposits have a fining upward sequence and were deposited on a sub-Eocene unconformity, with a maximum thickness of approximately 220 m (Lindgren, 1911; Cassel and Graham, 2011; Tipp and Gabet, 2020). The auriferous gravels were divided into two units based on lithology and texture and were labeled as upper and lower units (Lindgren, 1911; Yeend, 1974).

The upper unit is approximately 122 m in thickness and consists of finer-grained material with pebble-sized clasts (Lindgren, 1911; Yeend, 1974). The upper unit also contains an abundance of clay and silt beds. Most clasts within this unit are milky-white quartz and quartzite, while the sand and silt-sized grains are comprised of mostly quartz (Lindgren, 1911; Yeend, 1974). The upper unit is predominantly brown to reddish in color due to oxidation and weathering.

The lower unit is approximately 20-43 m in thickness and is poorly sorted compared to the upper unit (Lindgren, 1911; Yeend, 1974). The lower unit is imbricated and contains pebbles to boulders as large as 3 m in diameter (Lindgren, 1911; Yeend, 1974). The lower unit remains visibly different from the upper unit due to the bluish-gray tint, which was

caused by slate and phyllite clasts being preserved in reducing conditions below the water table (Yeend, 1974). The lower gravels contain a higher concentration of gold than the upper gravels (Lindgren, 1911; Yeend, 1974).

Due to a warm and wet Eocene climate in the Sierras, significant chemical weathering transformed most of the feldspars in the gravels into kaolinite clay, which weakened and disaggregated the granitic clasts within the Tertiary gravels (Cassel et al., 2012). This process resulted in poor representation of granitic clasts within the placer gold deposits. Therefore, placer gold deposits consist primarily of quartz-rich gravels and metamorphic clasts like phyllite and slate (Allen, 1929; Cassel and Graham, 2011; Mix et al., 2015). Due to kaolinization, hydraulic mining sediment (HMS) from the Sierras is expected to have a higher concentration of quartz than feldspar (Lindgren, 1911; Allen, 1929; Yeend, 1974; Bouse et al., 2010).

The Gold Rush and Hydraulic Mining

California's Gold Rush began after the discovery of gold near Coloma, California, in 1848 (Alpers, 2017). In 1852, sediment waste had yet to become an issue but became of great concern when the modern form of hydraulic mining was developed (Gilbert, 1917). This form of hydraulic mining makes use of a pressurized water cannon to excavate gold-bearing sediment (Thrush, 1968). In the Sierras, hydraulic gold mining targeted the Tertiary gravels by using water cannons to blast the placer deposits. The slurry produced from this process was then diverted into sluice boxes, which are boxes with an open sloping channel and some type of riffling on the bottom surface of the box (Kelly et al., 1995). A significant

portion of gold was removed from the gravel by gravity separation. However, some gold was too fine to be separated by this process; therefore, miners would line the sluice boxes with elemental mercury, which would alloy with gold to form an amalgam. The gold was then isolated by roasting the amalgam, which vaporized the mercury (Averill, 1946). The mercury used in the Sierra Nevada was mined in the Coast Ranges (Domagalski, 1998).

From the mid to late 1800s, about 1.2×10^7 kg of mercury were used in the Sierra Nevada mines (Alpers and Hunerlach, 2000). During each operating season, around 10-30% of the mercury in the sluices was lost, as it floured under the constant pounding of gravels and boulders (Alpers and Hunerlach, 2000). As a result, the Sierra Nevada mines washed not only hydraulic mining sediment but also mercury into the adjoining rivers and tributaries (Hunerlach et al., 1999). The mercury was carried downstream by binding to fine sediments, particularly clays, due to their high surface area reactivity (Kongchum et al., 2011).

As hydraulic mining became more common, increased sedimentation downstream of the Sierra Nevada proceeded to the Sacramento Valley (Gilbert, 1917). Between 1853 and 1884, hydraulic mining delivered approximately 1.067×10^9 m^3 of sediment to Sierra Nevada rivers (James et al., 2009). This sediment caused channel aggradation, which led to greater downstream flooding and other problems such as the 1861 flood that engulfed Sacramento, the wide distribution of mining debris over agricultural lands located on both sides of the Yuba River, and the pollution of the surrounding stream water rendering it unusable for agricultural and domestic utilization (Woodruff v. Bloomfield, 1884; James, 1989; Kelley, 1989).

Yolo Bypass

Sacramento is one of the most flood-prone cities in the United States (James and Singer, 2008). Due to the flood risk, levees, dams, weirs, and bypasses were constructed throughout the Sacramento Valley. The levees confine not only the flow but also the sediment, which causes channel aggradation wherein the riverbed rises relative to the floodplain (Wright and Schoellhamer, 2004). This aggradation caused additional flooding, and to counter this, in the 1930s, the Yolo Bypass was engineered to be a floodway for flows from the Sacramento River, the Feather River, the Sutter Bypass, the Knights Landing Ridge Cut, Cache Creek, and Putah Creek (Fig. 1) (Springborn et al., 2011). The bypass is approximately 66 km long, north to south, and has an area of about 240 km^2 (Springborn et al., 2011). The bypass is capped on the north side by the Fremont Weir. The western portion of the bypass has partial levees, while the east side is bordered by an extensive and complete levee system (California Department of Fish and Game, 2008). Most of the bypass consists of farms and grasslands, whereas to the south, the bypass becomes a more estuarine environment (California Department of Fish and Game, 2008). The south end of the bypass eventually drains back into the Sacramento River.

The floodwater from the Sutter Bypass and the Feather River mix with the Sacramento River in a convergence zone adjoining the Fremont Weir, and during flooding, the flow overtops the weir and is then distributed into Yolo Bypass (Singer et al., 2008). The flood flow carries hydraulic mining sediment and mercury, which get deposited throughout the basin. The converging flows in the Yolo Bypass are wide, shallow, and have a low gradient

4
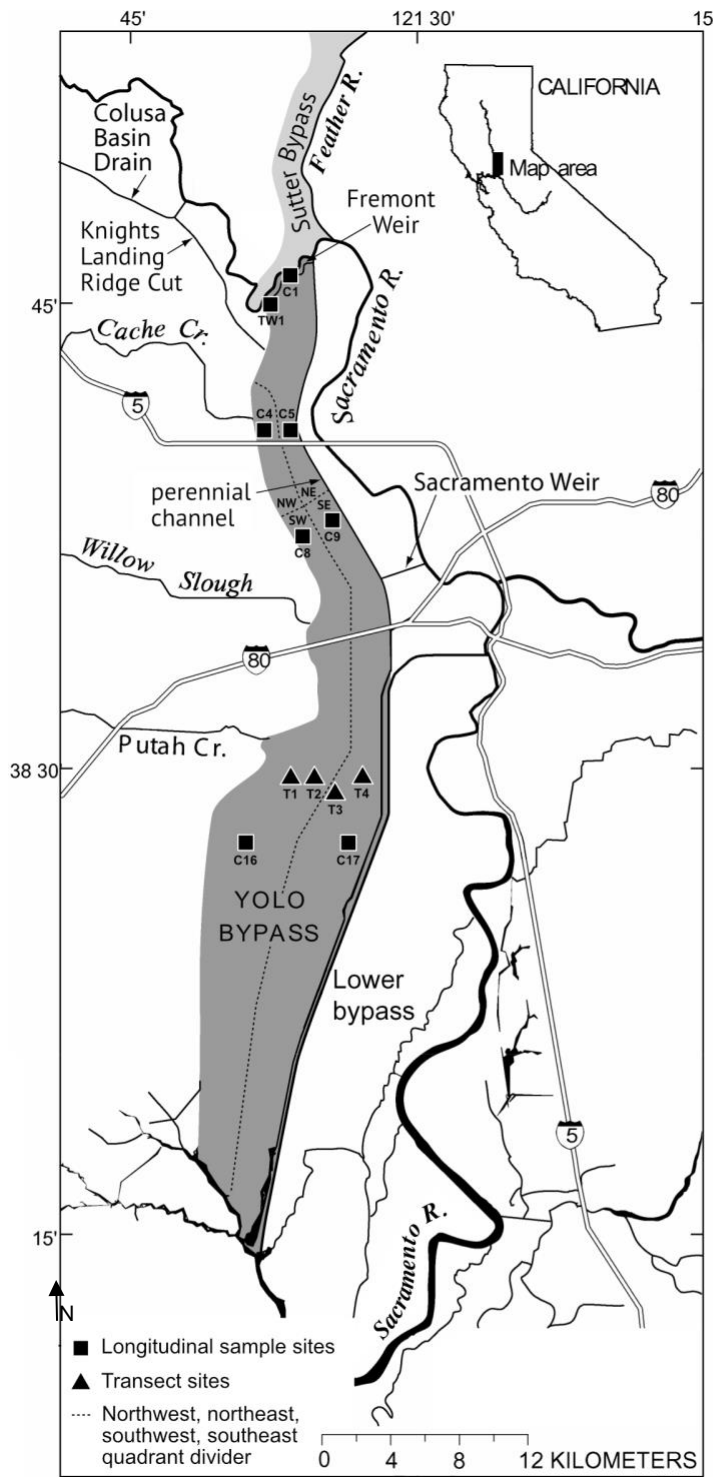
Figure 1. Map showing approximate locations of the four transect and eight longitudinal borehole sampling sites in the Yolo Bypass. Modified from Schemel et al. (2002).

and velocity, resulting in restrained mixing and banding of streams, a phenomenon called hydrologic banding (Sommer et al., 2008). Putah Creek bands the western side, Cache Creek and the Knights Landing Ridge Cut band the central part, and the Fremont Weir flow (Sutter Bypass, Feather River, and the Sacramento River) bands the eastern side of the bypass (Sommer et al., 2008). Cache Creek contributes 11% of the water, 38% of the sediment, and 64% of the mercury delivered to the bypass. In contrast, the Fremont Weir flow contributes 71% of the water, 47% of the sediment, and 31% of the mercury (Springborn et al., 2011).

Significance

The Yolo Bypass was created to offload floodwaters in the lower Sacramento area, though this is not its only use (Sommer et al., 2001). The bypass hosts farming, including the cultivation of white and wild rice, with floodwaters bringing in seasonal nutrients (Marvin-DiPasquale et al., 2013). The central region of the bypass is a wildlife habitat home to fish, birds, and other animals (California Department of Fish and Game, 2008). The Yolo Bypass is also used for recreational and educational purposes such as summer camps, hunting, bird watching, and guided tours. Hydraulic mining sediment and mercury from both the Coast Ranges and the Sierra Nevada affect these uses to some degree.

Inorganic mercury (Hg) can be transformed into an organic form of mercury, methylmercury ($MeHg^+$ or CH_3Hg^+), when certain bacteria are present in an anoxic sedimentary environment (Domagalski, 2001). Methylmercury is a reproductive and neurological toxin that is biologically hazardous (Bouse et al., 2010). Some studies have discovered higher concentrations of methylmercury in rice in regions contaminated with

mercury (e.g., Marvin-DiPasquale et al., 2013). Methylmercury is dangerous not only for fish and birds but also for fish-eating predators and humans who consume the contaminated rice and fish.

Goals of the Study

There were three goals for this study. The first goal was to determine the fraction of HMS for a given sample of Yolo Bypass sediment. This is important because knowing the location of high amounts of HMS could help in identifying Hg hotspots. To achieve the first goal, boreholes from the eastern quadrants in the Yolo Bypass were selected since that is the side with the sediment coming from the Sierra Nevada. The second goal was to determine if there were relationships between Hg concentrations and the geochemical and mineralogical signatures of HMS. Identifying these relationships is helpful because measuring Al/Ca, for example, is quicker and cheaper than measuring Hg. The third goal was to determine if hydraulic banding leaves a geochemical and mineralogical signature in the sediment. Understanding the chemical and mineralogical fingerprint of each band helps determine the origin of the sediment in the bypass as well as the amount of mixing between each band.

MATERIALS AND METHODS

Sample Collection

Twelve borehole sites were selected based on criteria such as ease of access, distance between sample site locations, and sites of interest, such as directly downstream of the primary bypass inputs (Fig. 1; Table 1). Four of the twelve borehole sites were chosen to obtain west-to-east chemical and mineralogical data. A total of 79 samples of sediment were taken from 12 borehole sites along the Yolo Bypass (Fig. 1). Tables 1 and 2 list borehole sample IDs, borehole locations, depth of the boreholes, date the core was collected, and number of samples collected from each borehole. To collect the samples from the boreholes, a stainless-steel closed bucket auger was used to minimize cross contamination. The stainless-steel auger was not ideal for studying trace elements as occasionally stainless-steel augers can be a source of trace metals (Valkovic, 1983; Shelton and Capel, 1994). Therefore, great care was taken to sample from the inner parts of the cores. Samples were taken at 1 m intervals and where noticeable changes occurred such as color or grain size, down to a maximum depth of 6 m. After the collection of each new sample, the auger was washed with deionized water. The samples were put in Ziploc bags, labeled, and sealed to prevent any cross-contamination.

Five additional samples consist of *in-situ* Tertiary gravels (Fig. 2; Table 2). Three of these samples came from the Blue Point Mine (BPM), located in Smartsville, California (Nakamura et al., 2018). The other two samples were collected in Sierra County, California, at the

Indian Hill hydraulic mining site. All five Tertiary *in-situ* gravel samples were used to provide

chemical and mineralogical baseline concentrations.

TABLE 1. YOLO BYPASS, SACRAMENTO, CALIFORNIA BOREHOLE DATA

Borehole identifier	Latitude	Longitude	Full name	Borehole Depth (cm)	Date	No. of samples
C1	38.76428	-121.64892	Core 01	406.0	8/9/16	6
C4	38.67618	-121.66690	Core 04	402.5	10/8/16	7
C5	38.67592	-121.64958	Core 05	409.0	10/8/16	6
C8	38.62568	-121.64328	Core 08	490.5	8/17/16	10
C9	38.63287	-121.62398	Core 09	139.0	8/16/16	4
T1	38.48589	-121.62967	Transect 1	373.0	5/15/17	6
T2	38.48573	-121.61951	Transect 2	300.0	5/16/17	5
T3	38.48220	-121.61272	Transect 3	402.0	5/15/17	5
T4	38.48570	-121.59963	Transect 4	399.0	5/15/17	7
C16	38.45936	-121.65891	Core 16	504.0	9/2/16	8
C17	38.45715	-121.60763	Core 17	368.0	8/26/16	9
TW1	38.75776	-121.66182	Tree Well 1	409.0	5/6/17	6

TABLE 2. BLUE POINT MINE, SMARTSVILLE, CALIFORNIA AND INDIAN HILL, SIERRA COUNTY, CALIFORNIA SAMPLE DATA

Sample identifier	Latitude	Longitude	Full name	Type	Date	No. of samples
IH_Tg Upper	39.50907	-121.00455	Indian Hills Tertiary Gravel Upper Unit	Outcrop	3/24/18	1
IH_Tg Lower	39.50907	-121.00455	Indian Hills Tertiary Gravel Lower Unit	Outcrop	3/24/18	1
M1 (BPM)	39.21004	-121.28429	Blue Point Mine 1	Outcrop	3/26/16	1
M2S (BPM)	39.20852	-121.28742	Blue Point Mine 2 Sandbar	Outcrop	3/26/16	1
M3S (BPM)	39.20822	-121.28853	Blue Point Mine 3 Sandbar	Outcrop	3/26/16	1
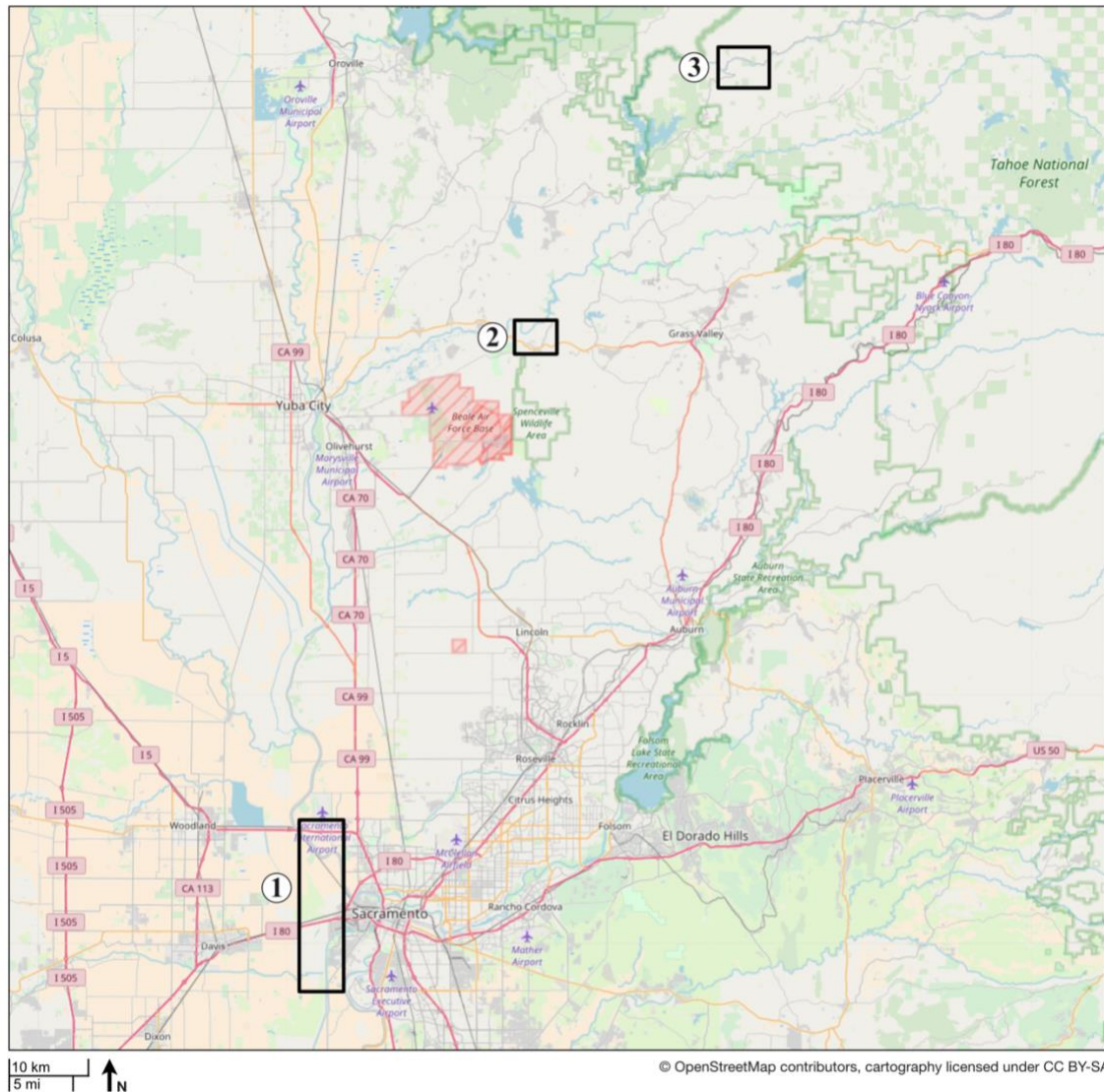
Figure 2. Map showing the locations of (1) Yolo Bypass, Sacramento, (2) Blue Point Mine, Smartsville and (3) Indian Hill, Sierra County. ©OpenStreetMap contributors (https://www.openstreetmap.org/copyright).

Mineralogical Analysis Using X-Ray Diffraction

X-ray diffraction (XRD) was used to quantify mineralogical and geochemical differences between pre-mining sediment and mining sediment. For bulk mineral analysis, 15 g of sediment per sample were put into weigh boats and dried at 80°F for three days. After the

samples were dried, they were homogenized using a mortar and pestle and each sample was entirely sieved to less than 150 μm (Jackson, 1985). All tools and sieves were cleaned by washing, rinsing with deionized water, and fully drying before use on each sample to prevent cross-contamination. Samples were side-packed into XRD sample holders to reduce the preferred orientation of mineral grains. The XRD patterns were obtained from the Rigaku SmartLab at NASA Ames Research Center. The XRD was used with CuK-alpha radiation at 40Kv and 40μA with divergence, scattering, and receiving slits set to ½°, ½°, and 0.3 mm, respectively. Patterns were collected from 2-65° [°2θ] at a step size of 0.02˚ for 8 seconds per step. Each sample's mineralogy was determined by using MDI Jade software and the ICDD PDF-2 database (Gates-Rector and Blanton, 2019). The quartz-to-plagioclase, Q/P, was calculated using a rietveld refinement in the program Profex (Doebelin and Kleeberg, 2015).

Fine-grained sediment from hydraulic mining was distributed at higher rates early in the hydraulic mining process due to the ease with which these finer sediments were carried over and washed out of overflowing sluices while the coarse-grained sediment stayed in the sluices or were deposited nearby (Bouse et al., 2010). Grain size distribution is an important factor when examining metals in sediment such as Hg, Pb, Ni, and Sr. Fine-grained sediment tends to have higher concentrations of heavy metals compared to coarse-grained sediment (Yu et al., 2012). The fine-grained sediments, such as clays, have high surface-to-volume ratios and higher adsorption capacities, while metals have an affinity for clays (McLean and Bledsoe, 1992). These finer grained sediments, or clays, tend to be sinks for heavy metals.

The types of clays within the bypass were analyzed using six samples from the transect cores, three with the highest Hg concentrations and three with the lowest Hg concentrations. To examine the interaction between clays and Hg in the bypass, these six samples underwent clay fraction separation to a fraction size of less than 2 micrometers followed by an ethylene glycol vapor treatment and placed in an oven, at 60 degrees Celsius, overnight (Poppe et al., 2001). Smectite can be identified at the diffraction angle [°2θ] 5.2. Kaolinite can be identified at the diffraction angle [°2θ] 12.4 and 25.1. Chlorite can be identified at the diffraction angle [°2θ] at 6.1, 12.4, 18.7, and 25.1. Illite can be identified at the diffraction angle [°2θ] at 8.73, 17.77, and 26.79 (Moore and Reynolds Jr., 1989). By using these diffraction angles, shifts in peaks can be identified (Figs. 3 and 4).

Aqua Regia - Hg Cold Vapor FIMS

A third-party lab, Actlabs, analyzed all the samples taken from the twelve boreholes and the in-situ Tertiary gravels using their 1G – Aqua Regio – HG cold vapor flow injection mercury system (FIMS) method (Actlabs, 2018). A Perkin Elmer FIMS 100 cold vapor Hg analyzer was used to identify mercury within the samples. To begin, approximately 0.5 grams of each sample was digested with aqua regia at 90°C (Actlabs, 2018). The resulting mixture was oxidized so that Hg would take on the stable divalent form, which was then reduced to a volatile free atomic state using stannous chloride. Next, argon was used to transport the Hg into an absorption cell, which was then placed in the light path of an atomic absorption spectrophotometer (Actlabs, 2018). Measurements of the amount of cell absorption were performed by using the flow injection technique. The total amount
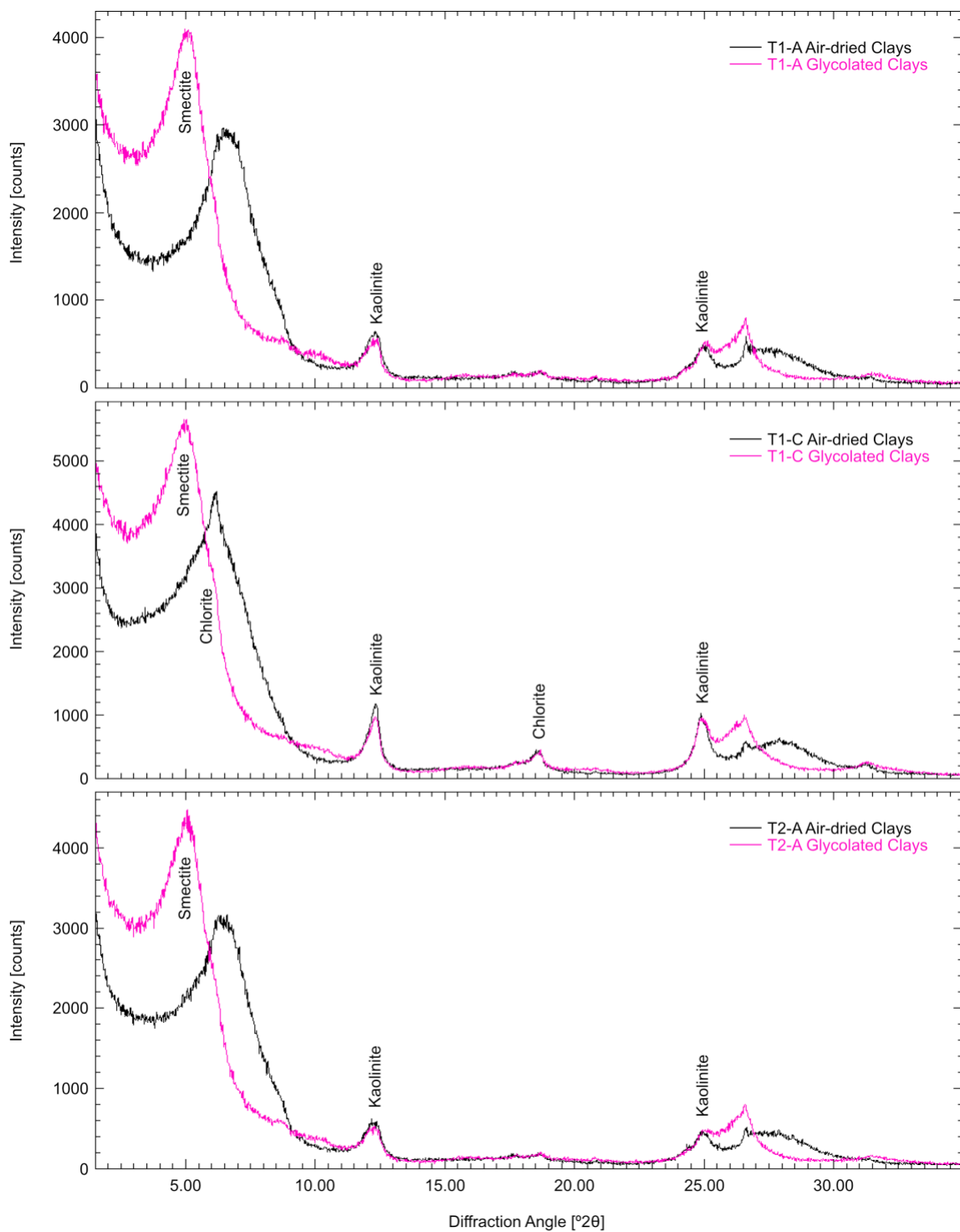
Figure 3. Graphs showing clay expansion in samples T1A, T1C, and T2A.
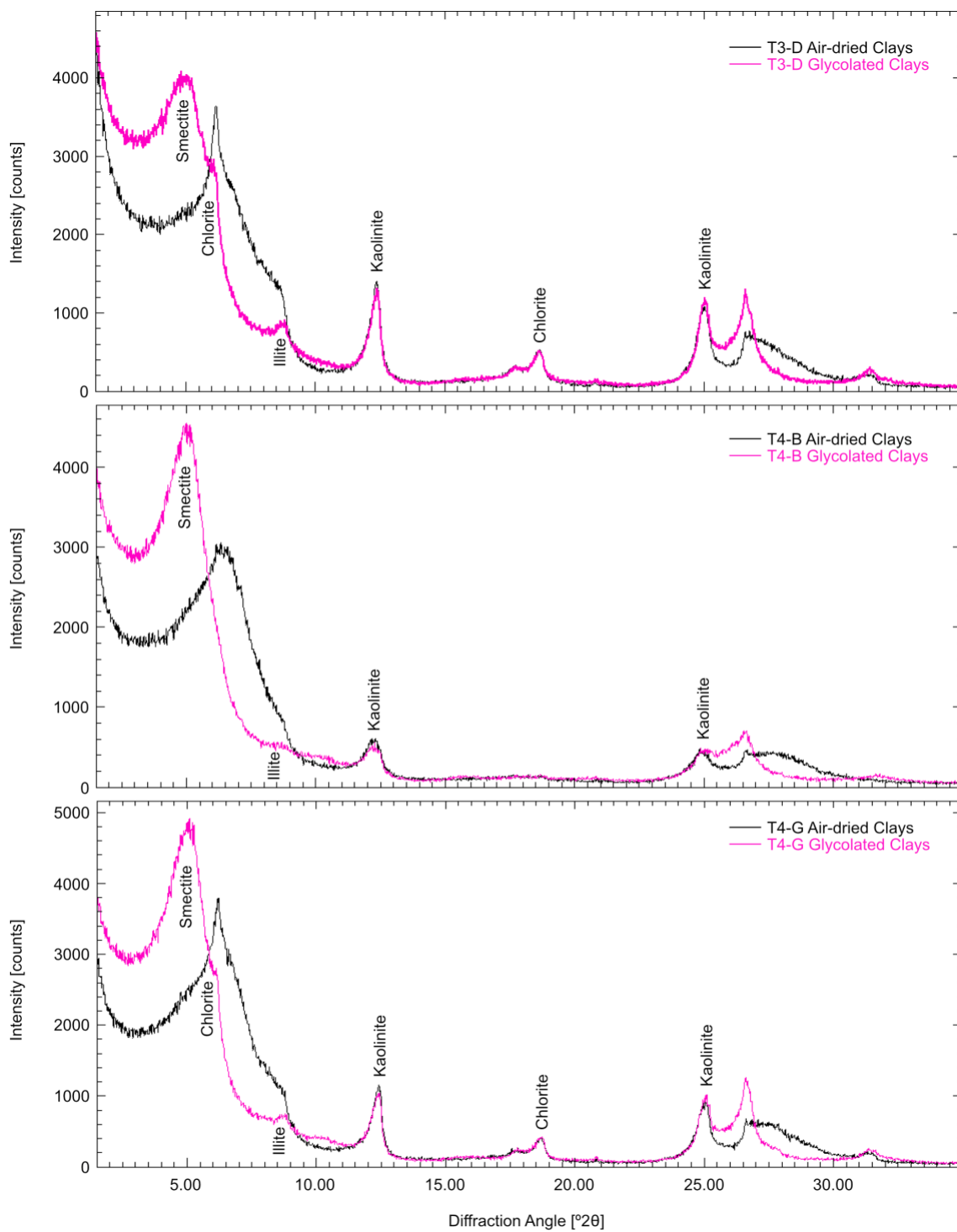
Figure 4. Graphs showing clay expansion in samples T3D, T4B, and T4G.

absorbed by the absorption cell, in the light path, is directly proportional to the concentration of mercury present.

Inductively Coupled Plasma-Optical Emission Spectroscopy (ICP-OES)

Actlabs analyzed the samples derived from the twelve boreholes and the five in-situ Tertiary gravels using their 4B – Lithium Metaborate/Tetraborate Fusion – Inductively Coupled Plasma method to determine the concentration of the major oxides in weight percent and trace elements in ppm: SiO_2, Al_2O_3, CaO, Fe_2O_3, K_2O, Sr, and Zr. Each individual sample was mixed with lithium metaborate and lithium tetraborate, after which it was placed and fused in an induction furnace (Actlabs, 2018). The resulting melts were directly poured, mixed, and dissolved into 5% nitric acid solutions, which contain an internal standard, cadmium, for calibration purposes. Then, each sample solution was analyzed for selected elements and oxides on a combination simultaneous-sequential Thermo Jarrell-Ash Enviro II ICP-OES or a Varian Vista 735 ICP-OES (Actlabs, 2018).

To evaluate the concentrations of the metals Pb and Ni in the samples, Actlabs recommended method 4B1 – Total Digestion – Inductively Coupled Plasma (ICP). For this method, 0.25 g of each sample underwent total digestion before being analyzed in the Varian Vista 735 ICP (Actlabs, 2018). Each sample was digested with hydrofluoric, nitric, and perchloric acids, after which they underwent several ramping and holding cycles to reach dryness. After the samples were digested and dried, they were brought back to solution with hydrochloric acid (Actlabs, 2018). Once in solution, these samples were analyzed with the Inductively Coupled Plasma-Optical Emission Spectroscopy method.

Geochemical Ratios and Clays

Four geochemical ratios examined in this study are Al/Ca, Al/K, Ca/Sr, and Ni/Zr. The Sierra Nevada is enriched in granitic rocks, which are partially comprised of feldspars (Bateman, 1992). Feldspars, which are easily weathered, release ions such as K^+, Na^+, and Ca^{2+}, followed by the precipitation of clay such as kaolinite (Blum, 1994). The aluminum in feldspars is a fairly immobile element and is relatively resistant to weathering, allowing for ratios such as Al/Ca and Al/K to be used as indicators for the intensity of weathering. When weathering intensity increases, Al/Ca and Al/K values increase in feldspar (Wei et al., 2006; Yang and Du, 2017).

The Tertiary gravels underwent intensive weathering, therefore sediment derived from the gravels should have high Al/Ca and Al/K values (Cassel et al., 2012). In contrast, modern sediment is less weathered and should have lower Al/Ca and Al/K values (Chapin III et al., 2011). In this study, Al/Ca and Al/K were primarily used to help determine the boundary between post-, contemporaneous, and pre-mining sediments as well as for identifying the Coast Ranges or the Sierra Nevada as the source of the sediment.

Granitic rocks are enriched in plagioclase and amphibole, which are two important carriers of Ca and Sr (Turner, 1899; Probst et al., 2000). Strontium and calcium both have similar hydrated ionic radius and charge. The Ca/Sr ratio is used primarily as a paleoclimate indicator (Pett-Ridge et al., 2009). During intense weathering Ca gets leached at higher rates than Sr, whereas Sr gets preferentially retained more strongly in the residual minerals and is more easily reincorporated in newly formed secondary minerals (Lucas et al., 1990). Greater

weathering intensity leads to less Ca and a lower Ca/Sr value (Pett-Ridge et al., 2009). Since

the Sierra Nevada underwent intense weathering during the Eocene, HMS is expected to

have a lower Ca/Sr value compared to modern sediment (Bouse et al., 2010; Cassel et al.,

2012). Sediment on the eastern portion of the Sacramento River floodplain has higher

concentrations of Ca and Sr when compared to the western portion of the Sacramento

River floodplain (Goldhaber et al., 2009). Therefore, the sediment coming from the Sierra

Nevada into the bypass should have higher concentrations of Ca and Sr when compared to

the sediment coming from the Coast Ranges into the bypass. Modern sediment, from the

Coast Ranges and Sierra Nevada, has the lowest Al/Ca values and highest Ca/Sr values,

making these two ratios useful for finding modern sediment in the Yolo Bypass (Bouse et al.,

2010). For this study Ca/Sr was primarily used to identify sediment as either pre-,

contemporaneous, or post-mining as well as to determine sediment as coming from either

the Coast Ranges or the Sierra Nevada. Determining sediment origins in the bypass was

simpler due to the little mixing that occurs between the four different flows.

The sediment in the Sacramento Valley is partially sourced from chemically and

mineralogically distinctive ultramafic rocks from the Coast Ranges ophiolite and, to a lesser

extent, the western metamorphic belt in the Sierra Nevada foothills (Morrison et al., 2009).

Hydrated ultramafic rocks are enriched in serpentine minerals which are the main source of

the trace element Ni (Morrison et al., 2009; Morrison et al., 2015). While olivine, the parent

rock to serpentinite, was the original Ni-bearing phase, serpentinization altered the olivine

into serpentine minerals such as antigorite, chrysotile and lizardite (Oze et al., 2004;

Morrison et al., 2015). Concentrations of Ni in Sacramento Valley sediments range from 65 to 224 mg/kg, whereas the typical U.S. soil concentration of Ni is 15 mg/kg (Morrison et al., 2015). Nickel concentrations are higher in the western Sacramento Valley compared to the eastern Sacramento Valley (Goldhaber at al., 2009; Morrison et al., 2009). The primary cause of lower concentrations of Ni on the eastern side when compared to the western side of Sacramento Valley is sediment dilution by granitic sources from the Sierra Nevada (Morrison et al., 2009). Due to erosion, weathering, and transportation of the Coast Ranges sediment, sediment in the western Sacramento Valley has greater concentrations of Ni relative to the eastern Sacramento Valley (Morrison et al., 2009). Sediment that contains Ni is transported from the Coast Ranges to the Yolo Bypass through Cache Creek and Putah Creek (Morrison et al., 2009).

Zircon is present in various igneous and metamorphic rocks (Fitzpatrick and Chittleborough, 2002). In parent rocks that are intensely weathered, there is an increase in Zr's relative abundance in the derived sediments (Fitzpatrick and Chittleborough, 2002). Zirconium is a relatively immobile element throughout weathering, alterations, and following intrusive, deformational, and metamorphic events (Petersen, 1983). The Zr concentrations in soil samples, are similar between the Coast Ranges, the Sacramento Valley, and the Sierra Nevada (Bradford et al., 1996). Zircon was used to normalize Ni in this study.

When compared to sediment from the Sierra Nevada, sediment from the Coast Ranges is enriched in more Ni (Goldhaber et al., 2009; Morrison et al., 2009). Therefore, sediment

in the western quadrants of the Yolo Bypass is expected to have higher concentrations of Ni when compared to the eastern quadrants of the bypass. Because of the differences of Ni in the Sacramento Valley, Ni/Zr would help distinguish sediment from either the Sierra Nevada or the Coast Ranges. Bouse et al. (2010) found that HMS has lower Ni/Zr values. For this study, Ni/Zr is used to differentiate sediment coming from either the Coast Ranges or Sierra Nevada, as well as to identify sediment as either pre-, contemporaneous, or post-mining.

Statistical Tests

In this study, the Yolo Bypass was divided into four quadrants: borehole C4 is located in the northwest quadrant, boreholes TW1, C1, C5 in the northeast quadrant, boreholes C8, T1, T2, C16 in the southwest quadrant, and boreholes C9, T3, T4, C17 in the southeast quadrant (Fig. 1). The geochemical concentrations, oxide percentages, and ratios were compared between each quadrant. To determine if there was any relationship between the geochemical composition of the cores and the location of the cores within the bypass, statistical tests were performed. A single factor ANOVA test was completed for each quadrant to determine if there is a relationship between quadrant location and Hg, Pb, Fe_2O_3, quartz-to-plagioclase, Al/Ca, Al/K, Ca/Sr, and Ni/Zr. The ANOVA tests were used to establish if the null hypothesis is true or false. In this study, the null hypothesis was that geochemical concentrations, oxide percentages, and ratio values occurred by chance in each quadrant location and were independent of those locations within the bypass. A significance level value of 0.05 was used.

However, to make the ANOVA tests more accurate, the outliers in the data needed to be removed since they could skew the results (Crain and Lysy, 2016). To determine if a value was an outlier, a box-and-whisker plot was used (Fig. 5). The box-and-whisker plot shows five different values, the maximum, the minimum, the 1st, 2nd or median, and the 3rd quartile. The interquartile value is the difference between the first and third quartile. A data point was determined to be an outlier if it exceeded a distance of 1.5 times the interquartile value range below or above the first and third quartile, respectively (Crain and Lysy, 2016). Those outliers were then removed from the data, and a second ANOVA test was performed.
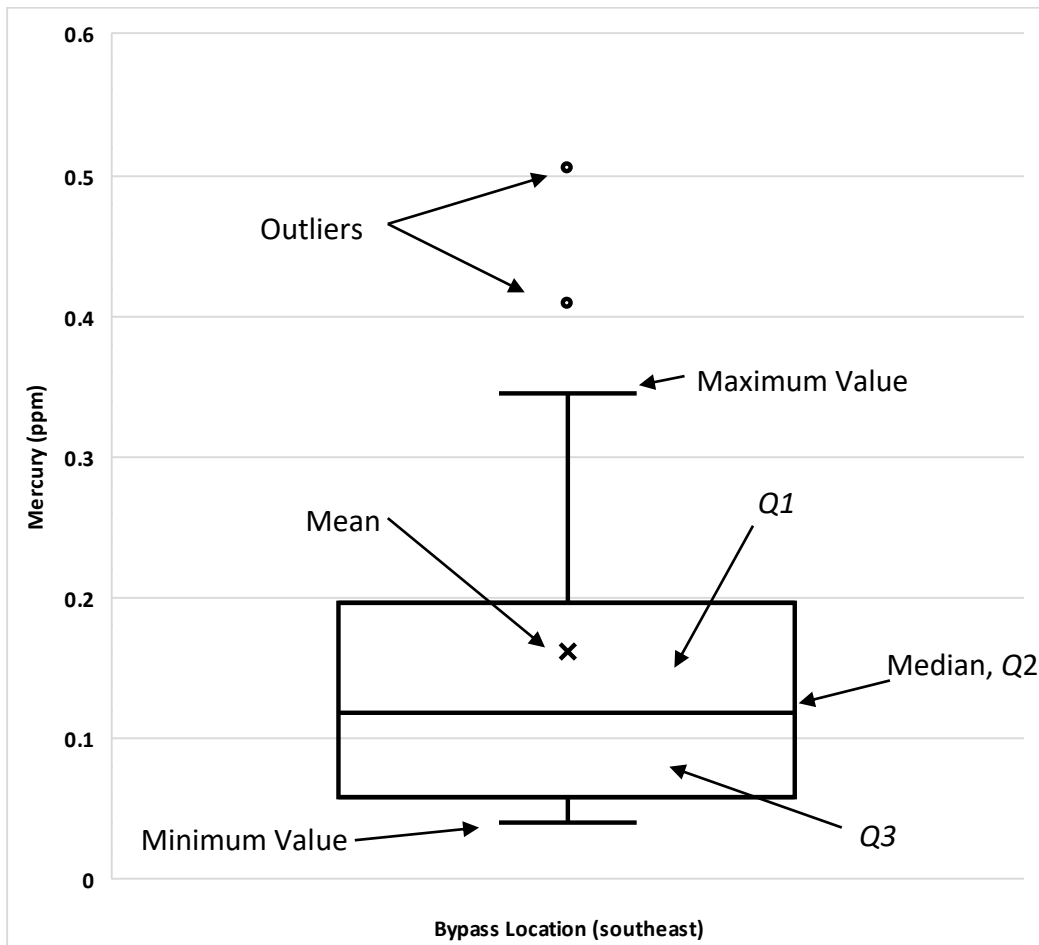
Figure 5. Box-and-whisker plot with labels.

A T-test of unequal variances was performed for Hg, Pb, Fe_2O_3, CaO, Q/P, Al/Ca, Al/K, Ca/Sr, and Ni/Zr to determine if the means were significantly different with respect to the eastern and western quadrants of the bypass. The alpha value used to determine significance was 0.05.

End-Member Mixing Analysis

An end-member mixing analysis (EMMA) was performed to calculate the proportions of HMS in any given sample from the eastern quadrants in the bypass. An EMMA consists of solving an equation to determine the proportions of the known end-members; in this case there are two end-members, pre-mining sediment and HMS. The equations used were:

$$x + y = z \tag{1}$$

$$(A \times x) + (B \times y) = (C \times z) \tag{2}$$

$$x = z \times \frac{C-B}{A-B} \times 100 \tag{3}$$

where x is the fraction of HMS, y is the fraction of pre-mining sediment, z is set equal to 1 assuming there are no other sediment sources, A is the Indian Hill end-member concentration, B is the pre-mining sediment end-member concentration, and C is the total sample concentration. In the EMMA equation the pre-mining sample averages were used as one end-member and the Indian Hill sample averages were used as the second end-member. Tracers used for this EMMA are geochemical values that show a distinction between pre-, contemporaneous, and post-mining sediment. The tracers used for end-

member values were CaO and Ca/Sr, since Ca is a common tracer used in most EMMA

studies (Barthold et al., 2011).

RESULTS

General Geochemistry

All 84 samples were analyzed for their concentrations and oxide percentages of Pb, Sr,

Hg, Zr, Ni, SiO_2, Al_2O_3, Fe_2O_3, CaO, and K_2O (Table 3). The depth profiles from each borehole

core are presented in Appendix 2.

TABLE 3. GEOCHEMICAL DATA FOR SAMPLES COLLECTED IN THE YOLO BYPASS, BLUE POINT MINE, AND INDIAN HILL

Sample identifier	Depth (cm)	[Hg] (ppm)	SiO_2 (%)	Al_2O_3 (%)	Fe_2O_3 (%)	CaO (%)	K_2O (%)	[Sr] (ppm)	[Zr] (ppm)	[Ni] (ppm)	[Pb] (ppm)
TWI-A	20.0	0.054	58.90	14.22	6.29	2.26	1.31	179	94	103	7
TWI-B	116.0	0.049	64.17	13.56	6.09	2.36	1.14	191	117	102	6
TWI-C	208.0	0.076	57.17	15.40	7.43	1.59	1.47	141	105	151	7
TWI-D	218.0	0.081	58.47	14.92	7.40	1.48	1.43	141	111	156	8
TWI-E	307.0	0.057	57.72	15.34	7.51	2.87	1.32	196	110	123	9
TWI-F	409.0	0.055	58.94	15.26	7.21	2.55	1.31	182	117	121	7
C1-A	33.0	0.150	58.84	14.77	6.70	1.69	1.32	141	87	114	10
C1-B	98.0	0.093	56.98	16.21	8.30	1.30	1.72	118	117	153	10
C1-C	212.0	0.062	61.62	13.91	6.43	1.80	1.33	160	93	160	7
C1-D	269.5	0.049	65.65	13.42	6.18	1.97	1.33	169	105	142	< 5
C1-E	303.5	0.035	66.18	12.25	5.45	2.15	1.21	168	73	120	6
C1-F	406.0	0.034	64.85	13.36	5.94	2.42	1.22	193	117	108	6
C4-A	24.0	0.333	56.93	14.68	7.40	1.39	1.48	133	94	214	16
C4-B	100.5	0.071	51.17	16.29	8.51	1.03	1.63	131	86	187	12
C4-C	203.0	0.086	52.26	16.65	8.57	1.36	1.58	146	94	186	< 5
C4-D	311.0	0.068	56.82	15.33	7.59	1.09	1.43	138	102	199	9
C4-E	356.0	0.071	57.05	15.52	7.14	1.02	1.40	142	95	195	11
C4-F	402.5	0.124	56.85	14.24	6.61	2.43	1.35	177	106	196	10
C4-G	495.0	0.114	55.32	11.80	6.19	4.88	1.10	257	95	210	7
C5-A	33.0	0.067	53.05	16.75	8.68	1.59	1.52	171	119	199	9
C5-B	100.0	0.056	57.47	14.98	7.42	1.41	1.40	160	125	194	10
C5-C	138.0	0.063	58.00	15.18	7.30	2.00	1.39	174	126	190	10
C5-D	206.0	0.094	61.57	14.32	6.91	1.13	1.43	148	113	211	10
C5-E	314.0	0.067	46.10	13.53	6.96	6.85	1.38	392	93	174	8
C5-F	409.0	0.127	51.47	14.55	7.19	3.14	1.51	252	84	208	10

TABLE 3. (CONTINUED)

Sample identifier	Depth (cm)	[Hg] (ppm)	SiO$_2$ (%)	Al$_2$O$_3$ (%)	Fe$_2$O$_3$ (%)	CaO (%)	K$_2$O (%)	[Sr] (ppm)	[Zr] (ppm)	[Ni] (ppm)	[Pb] (ppm)
C8-A	30.0	0.289	54.76	15.26	7.88	1.18	1.49	128	91	203	10
C8-B	102.0	0.151	53.20	15.23	7.99	1.02	1.53	133	98	209	13
C8-C	174.0	0.064	57.06	14.73	7.20	1.78	1.29	175	102	211	10
C8-D	199.0	0.060	58.68	14.35	6.51	2.26	1.22	200	109	188	8
C8-E	214.0	0.061	59.43	13.70	6.16	2.73	1.20	205	107	186	10
C8-F	308.5	0.107	62.74	13.04	6.32	1.18	1.28	142	102	232	7
C8-G	382.0	0.199	64.10	13.37	6.31	1.04	1.24	136	117	218	7
C8-H	405.0	0.145	65.92	12.18	6.47	1.23	1.31	137	125	244	7
C8-I	457.0	0.158	65.13	12.56	6.75	1.16	1.33	136	111	289	8
C8-J	490.0	0.209	61.81	13.83	6.88	1.12	1.29	131	138	211	9
C9-A	36.0	0.153	50.47	16.41	9.11	1.45	1.51	131	82	195	14
C9-B	57.0	0.154	50.85	16.97	9.58	1.49	1.55	134	98	191	13
C9-C	120.0	0.200	53.67	16.56	8.56	1.31	1.50	138	102	194	16
C9-D	139.0	0.171	61.49	14.00	7.35	1.26	1.29	154	102	199	10
T1-A	20.0	1.320	56.90	14.78	7.27	1.20	1.64	132	113	253	12
T1-B	107.0	0.070	60.77	13.99	6.26	0.92	1.21	139	133	219	9
T1-C	138.0	0.060	61.12	13.94	6.15	1.04	1.14	168	135	215	7
T1-D	208.0	0.202	59.73	14.20	6.55	1.31	1.45	167	130	227	8
T1-E	302.0	0.072	55.60	14.94	7.21	1.87	1.63	187	117	195	6
T1-F	373.0	0.114	60.78	13.85	6.55	1.62	1.51	161	133	196	8
T2-A	26.0	1.060	57.04	14.65	7.13	1.14	1.70	129	111	253	9
T2-B	104.0	0.219	55.02	15.01	7.46	1.03	1.66	117	103	265	10
T2-C	201.0	0.089	58.43	14.30	6.70	1.12	1.33	147	119	223	9
T2-D	250.0	0.085	59.66	13.94	6.26	1.88	1.26	180	135	193	6
T2-E	300.0	0.293	60.79	14.43	7.40	0.99	1.38	137	239	260	7
T3-A	14.0	0.506	54.67	15.31	7.40	1.10	1.53	124	112	241	12
T3-B	102.0	0.122	58.19	14.96	6.90	1.04	1.35	129	125	216	10
T3-C	191.0	0.054	59.95	14.00	5.86	1.63	1.22	175	134	172	7
T3-D	290.0	0.047	50.02	15.05	7.45	3.69	1.66	206	105	189	< 5
T3-E	402.0	0.050	55.09	16.07	7.38	1.64	1.69	137	113	155	6
T4-A	15.0	0.345	51.34	16.70	8.10	1.24	1.50	120	108	237	12
T4-B	108.0	0.508	55.88	15.71	7.54	1.40	1.53	131	114	198	11
T4-C	159.0	0.208	50.47	17.36	8.24	1.22	1.58	118	100	246	9
T4-D	208.0	0.076	54.30	15.79	8.29	1.13	1.43	113	119	221	10
T4-E	292.0	0.058	54.02	14.97	7.36	2.43	1.40	177	119	191	6
T4-F	323.0	0.049	47.67	13.30	6.47	7.31	1.21	334	103	139	8
T4-G	399.0	0.040	57.87	15.57	7.45	1.87	1.45	158	118	141	7

TABLE 3. (CONTINUED)

Sample identifier	Depth (cm)	[Hg] (ppm)	SiO_2 (%)	Al_2O_3 (%)	Fe_2O_3 (%)	CaO (%)	K_2O (%)	[Sr] (ppm)	[Zr] (ppm)	[Ni] (ppm)	[Pb] (ppm)
C16-A	22.5	0.064	57.16	14.46	7.47	1.14	1.36	134	99	269	11
C16-B	77.5	0.134	59.74	13.09	6.80	1.06	1.33	153	101	267	9
C16-C	108.5	0.095	59.62	12.37	6.16	1.90	1.29	189	92	237	7
C16-D	171.0	0.240	64.14	12.28	6.33	1.13	1.34	137	147	286	7
C16-E	204.5	0.106	59.76	13.13	6.29	2.20	1.27	154	123	216	9
C16-F	302.5	0.115	62.43	13.87	6.06	1.35	1.23	156	120	205	8
C16-G	399.0	0.138	55.80	15.42	7.38	1.63	1.66	148	97	223	9
C16-H	504.0	0.114	58.24	13.40	6.17	2.91	1.38	209	113	187	9
C17-A	19.0	0.410	54.65	15.17	7.34	1.36	1.50	134	89	186	13
C17-B	105.0	0.118	53.32	14.40	7.01	2.79	1.28	218	95	240	6
C17-C	135.0	0.108	55.88	14.38	6.86	2.26	1.34	186	99	242	10
C17-D	215.0	0.137	57.90	14.28	6.61	1.20	1.38	147	96	228	10
C17-E	278.0	0.089	63.14	13.83	6.33	1.27	1.19	168	165	180	10
C17-F	310.0	0.086	59.98	14.11	7.12	1.50	1.26	191	117	223	10
C17-G	317.0	0.082	56.42	14.69	6.77	2.51	1.34	195	111	208	10
C17-H	329.5	0.193	51.49	11.65	5.92	6.54	1.01	289	93	158	8
C17-I	368.0	0.060	53.49	12.91	6.10	5.57	1.00	322	99	128	8
IH_Tg Upper	N.A.	0.021	67.77	14.22	8.32	0.22	1.32	35	195	191	13
IH_Tg Lower	N.A.	0.098	68.82	15.36	3.88	0.29	1.28	41	204	165	11
M1(BPM)	N.A.	0.051	64.99	15.15	4.82	1.27	1.87	264	133	32	12
M2S (BPM)	N.A.	0.013	64.29	15.71	5.37	0.86	2.08	149	578	36	14
M3S (BPM)	N.A.	0.010	72.98	12.42	3.11	0.80	1.97	138	124	19	13

N.A. = not applicable.

Lead concentrations in the core samples range from <5 to 16 ppm with a limit of detection (LOD) of 5 ppm. The average of all the Pb concentrations in the core samples is 8.9 ± 2.3 ppm. Although highly variable the abundance of Pb concentration in the Earth's crust is approximately 15 ppm (Kabata-Pendias, 2001). Out of the 12 cores, seven contain samples with the highest Pb concentration in the top 50 cm of the core. The Yolo Bypass was divided into four quadrants, the northwest, northeast, southwest, and southeast (Fig. 1). The northwest quadrant contains the highest average Pb concentration compared to the

other quadrants (Fig. 6). Core T4 has the highest average Pb concentration compared to the rest of the transect cores (Fig. 7). Only one ANOVA test was performed, as there were no outliers. Lead concentrations from all core samples within the northwest, northeast, southwest, and southeast quadrants were used in the ANOVA test. There were no significant differences in mean Pb concentration between quadrants. The Indian Hill upper- and lower- unit *in-situ* samples have Pb concentrations of 13 and 11 ppm, respectively.
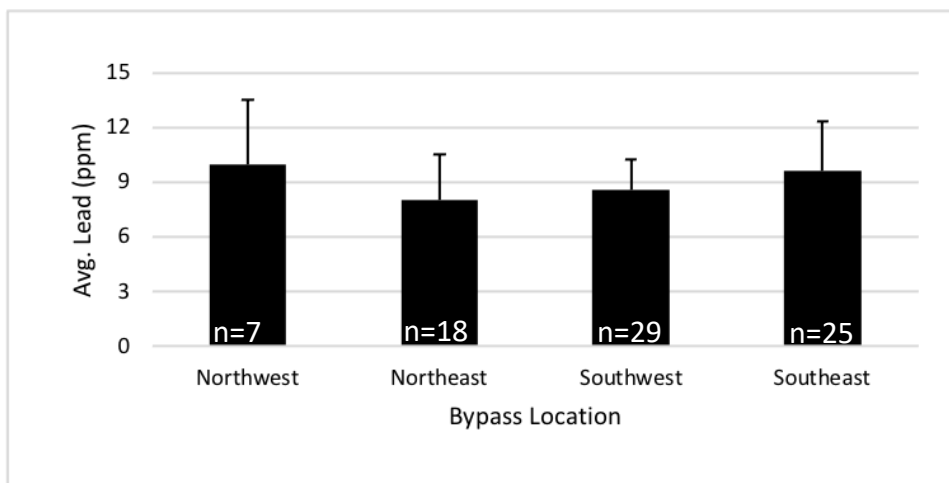
Figure 6. Average Pb concentration for each quadrant (n= samples that were averaged).
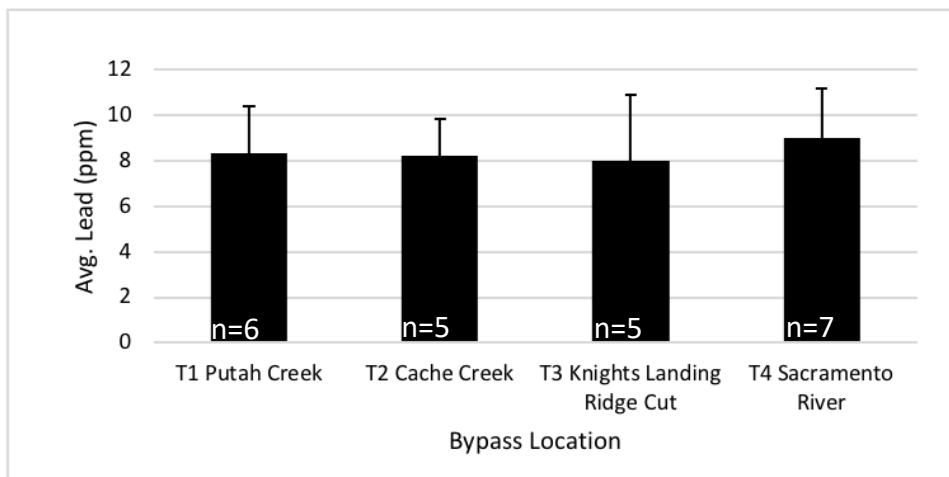
Figure 7. Average Pb concentration for the transect cores.

Strontium concentrations in the core samples range from 113 ppm to 392 ppm with an LOD of 2 ppm (Actlabs, 2018). The average concentration for Sr in the core samples is 167 ± 49.6 ppm. The Indian Hill Tertiary *in-situ* upper- and lower-unit samples have Sr concentrations of 35 ppm and 41 ppm, respectively. Zr concentrations in the core samples range from 73 ppm to 239 ppm with an LOD of 2 ppm (Actlabs, 2018). The average concentration of Zr in the core samples is 111 ± 21.5 ppm. The Indian Hill Tertiary *in-situ* upper- and lower-unit samples have Zr concentrations of 195 ppm and 204 ppm, respectively. Ni concentrations in the core samples range from 102 ppm to 289 ppm with an LOD of 2 ppm (Actlabs, 2018). The average concentration of Ni in the core samples is 198 ± 42.5 ppm. The Indian Hill Tertiary *in-situ* upper- and lower-unit samples have Ni concentrations of 191 ppm and 165 ppm, respectively.

The iron oxide weight percent in the core samples ranges from 5.5% to 9.6%, with a LOD of 0.01% (Actlabs, 2018). The average weight percent of Fe_2O_3 in the core samples is 7.1% ± 0.8%. The southeast quadrant contains the highest average weight percent of Fe_2O_3 in the core samples compared to the rest of the quadrants' core samples (Fig. 8). Of the four transect cores, T4 has the highest average weight percent of Fe_2O_3 (Fig. 9). Two ANOVA tests were performed, one with outliers and one without outliers, between the average weight percent of Fe_2O_3 in the quadrants of the bypass. A T-test was performed between the average weight percent of Fe_2O_3 in the bypass's western and eastern cores. There were no significant differences in mean Fe_2O_3 weight percent between quadrants or between the

bypass's western and eastern cores. The Indian Hill Tertiary *in-situ* upper- and lower-unit samples have a weight percent of Fe_2O_3 at 8.3% and 3.9%, respectively.
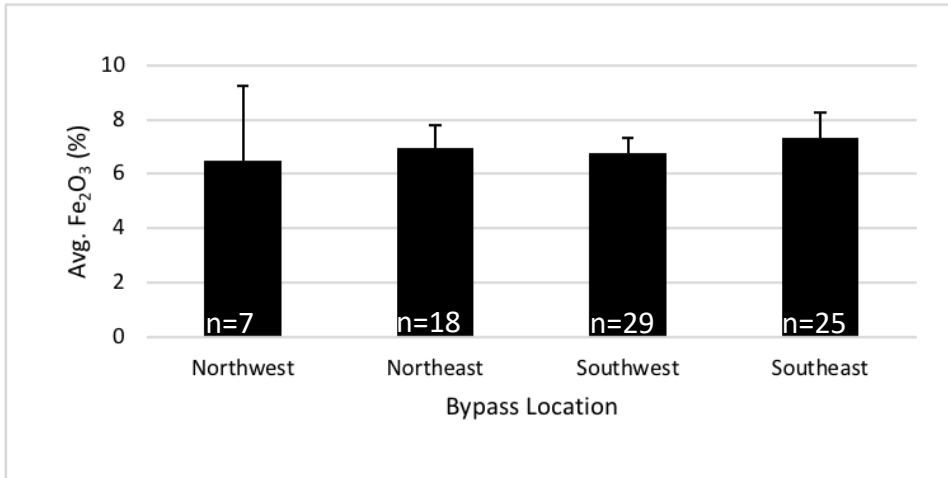
Figure 8. Average iron oxide (%) for each quadrant.
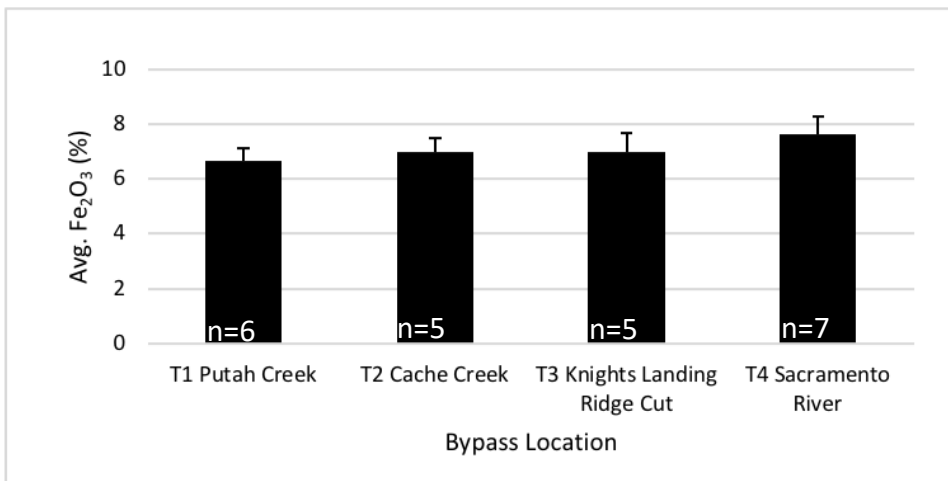
Figure 9. Average iron oxide (%) for the transect cores.

The weight percentages of silicon dioxide, in the core samples, range from 46% to 66% with a LOD of 0.01% (Actlabs, 2018). The average weight percent, in the core samples, of SiO_2 is 57% ± 4.4%. The weight percent of SiO_2 for Indian Hill Tertiary *in-situ* upper- and lower-unit samples are 68% and 69%, respectively. Potassium oxide ranges from 1.0% to

1.7% with a LOD of 0.01% (Actlabs, 2018). The average weight percent, in the core samples, of K_2O is 1.4% ± 0.16%. The weight percentages of K_2O for Indian Hill Tertiary *in-situ* upper- and lower-unit samples are 1.3% and 1.3%, respectively. Aluminum oxide ranges from 11.7% to 17.4% with a LOD of 0.01% (Actlabs, 2018). The average weight percent, in the core samples, of Al_2O_3 is 14.5% ± 1.2%. The weight percentages of Al_2O_3 for Indian Hill Tertiary *in-situ* upper- and lower-unit samples are 14% and 15%, respectively.

Calcium oxide ranges from 0.8% to 7.3% with a LOD of 0.01% (Actlabs, 2018). The average weight percent, in the core samples, of CaO is 1.9% ± 1.3. The weight percentages of CaO for Indian Hill Tertiary *in-situ* upper- and lower-unit samples are 0.2% and 0.3%, respectively. Calcium oxide weight percent means were analyzed for significance regarding the eastern or western quadrants. The T-test for CaO provided a two-tailed P-value of 0.0006, which is lower than the alpha value of 0.05 and, therefore, the mean differences are significant regarding the eastern and western quadrants in the bypass.

The values for Al/Ca, Al/K, Ca/Sr, and Ni/Zr in the core samples were calculated (Table 4). In the core samples from the bypass, the values for Al/Ca range from 1.8 to 15.2, The average value in the core samples for Al/Ca is 9.5 ± 3.7. In the core samples from the bypass, the values for Al/K range from 8.6 to 12.2. The average value in the core samples for Al/K is 10.5 ± 0.84. In the core samples from the bypass, the values for Ca/Sr range from 0.62 to 2.26. The average value in the core samples for Ca/Sr is 1.08 ± 0.33. In the core samples from the bypass, the values for Ni/Zr range from 0.87 to 2.72. The average value in the core samples for Ni/Zr is 1.82 ± 0.44. The northwest quadrant has the highest average

TABLE 4. GEOCHEMICAL RATIOS

Sample identifier	Depth (cm)	Al/Ca	Al/K	Ni/Zr	Ca/Sr
TWI-A	20.0	6.29	10.85	1.10	1.26
TWI-B	116.0	5.75	11.89	0.87	1.24
TWI-C	208.0	9.69	10.48	1.44	1.13
TWI-D	218.0	10.08	10.43	1.41	1.05
TWI-E	307.0	5.34	11.62	1.12	1.46
TWI-F	409.0	5.98	11.65	1.03	1.40
C1-A	33.0	8.74	11.19	1.31	1.20
C1-B	98.0	12.47	9.42	1.31	1.10
C1-C	212.0	7.73	10.46	1.72	1.13
C1-D	269.5	6.81	10.09	1.35	1.17
C1-E	303.5	5.70	10.12	1.64	1.28
C1-F	406.0	5.52	10.95	0.92	1.25
C4-A	24.0	10.56	9.92	2.28	1.05
C4-B	100.5	15.82	9.99	2.17	0.79
C4-C	203.0	12.24	10.54	1.98	0.93
C4-D	311.0	14.06	10.72	1.95	0.79
C4-E	356.0	15.22	11.09	2.05	0.72
C4-F	402.5	5.86	10.55	1.85	1.37
C4-G	495.0	2.42	10.73	2.21	1.90
C5-A	33.0	10.53	11.02	1.67	0.93
C5-B	100.0	10.62	10.70	1.55	0.88
C5-C	138.0	7.59	10.92	1.51	1.15
C5-D	206.0	12.67	10.01	1.87	0.76
C5-E	314.0	1.98	9.80	1.87	1.75
C5-F	409.0	4.63	9.64	2.48	1.25
C8-A	30.0	12.93	10.24	2.23	0.92
C8-B	102.0	14.93	9.95	2.13	0.77
C8-C	174.0	8.28	11.42	2.07	1.02
C8-D	199.0	6.35	11.76	1.72	1.13
C8-E	214.0	5.02	11.42	1.74	1.33
C8-F	308.5	11.05	10.19	2.27	0.83
C8-G	382.0	12.86	10.78	1.86	0.76
C8-H	405.0	9.90	9.30	1.95	0.90
C8-I	457.0	10.83	9.44	2.60	0.85
C8-J	490.0	12.35	10.72	1.53	0.85

TABLE 4. (CONTINUED)

Sample identifier	Depth (cm)	Al/Ca	Al/K	Ni/Zr	Ca/Sr
C9-A	36.0	11.32	10.87	2.38	1.11
C9-B	57.0	11.39	10.95	1.95	1.11
C9-C	120.0	12.64	11.04	1.90	0.95
C9-D	139.0	11.11	10.85	1.95	0.82
T1-A	20.0	12.32	9.01	2.24	0.91
T1-B	107.0	15.21	11.56	1.65	0.66
T1-C	138.0	13.40	12.23	1.59	0.62
T1-D	208.0	10.84	9.79	1.75	0.78
T1-E	302.0	7.99	9.17	1.67	1.00
T1-F	373.0	8.55	9.17	1.47	1.01
T2-A	26.0	12.85	8.62	2.28	0.88
T2-B	104.0	14.57	9.04	2.57	0.88
T2-C	201.0	12.77	10.75	1.87	0.76
T2-D	250.0	7.41	11.06	1.43	1.04
T2-E	300.0	14.58	10.46	1.09	0.72
T3-A	14.0	13.92	10.01	2.15	0.89
T3-B	102.0	14.38	11.08	1.73	0.81
T3-C	191.0	8.59	11.48	1.28	0.93
T3-D	290.0	4.08	9.07	1.80	1.79
T3-E	402.0	9.80	9.51	1.37	1.20
T4-A	15.0	13.47	11.13	2.19	1.03
T4-B	108.0	11.22	10.27	1.74	1.07
T4-C	159.0	14.23	10.99	2.46	1.03
T4-D	208.0	13.97	11.04	1.86	1.00
T4-E	292.0	6.16	10.69	1.61	1.37
T4-F	323.0	1.82	10.99	1.35	2.19
T4-G	399.0	8.33	10.74	1.19	1.18
C16-A	22.5	12.68	10.63	2.72	0.85
C16-B	77.5	12.35	9.84	2.64	0.69
C16-C	108.5	6.51	9.59	2.58	1.01
C16-D	171.0	10.87	9.16	1.95	0.82
C16-E	204.5	5.97	10.34	1.76	1.43
C16-F	302.5	10.27	11.28	1.71	0.87
C16-G	399.0	9.46	9.29	2.30	1.10
C16-H	504.0	4.60	9.71	1.65	1.39

TABLE 4. (CONTINUED)

Sample identifier	Depth (cm)	Al/Ca	Al/K	Ni/Zr	Ca/Sr
C17-A	19.0	11.15	10.11	2.09	1.01
C17-B	105.0	5.16	11.25	2.53	1.28
C17-C	135.0	6.36	10.73	2.44	1.22
C17-D	215.0	11.90	10.35	2.38	0.82
C17-E	278.0	10.89	11.62	1.09	0.76
C17-F	310.0	9.41	11.20	1.91	0.79
C17-G	317.0	5.85	10.96	1.87	1.29
C17-H	329.5	1.78	11.53	1.70	2.26
C17-I	368.0	2.32	12.91	1.29	1.73
IH_Tg Upper	N.A.	64.64	10.77	0.98	0.63
IH_Tg Lower	N.A.	52.97	12.00	0.81	0.71
M1 (BPM)	N.A.	11.93	8.10	0.24	0.48
M2S (BPM)	N.A.	18.27	7.55	0.06	0.58
M3S (BPM)	N.A.	15.53	6.30	0.15	0.58

N.A. = not applicable.

Al/Ca and Ni/Zr values, while the northeast has the highest average Ca/Sr values, and the southeast quadrant has the lowest average Al/K values (Figs. 10, 12, 14, and 16). The transect core T2 contains the highest average Al/Ca and Ni/Zr values, while transect core T4 has the highest averages of Al/K and Ca/Sr values (Figs. 11, 13, 15, and 17).
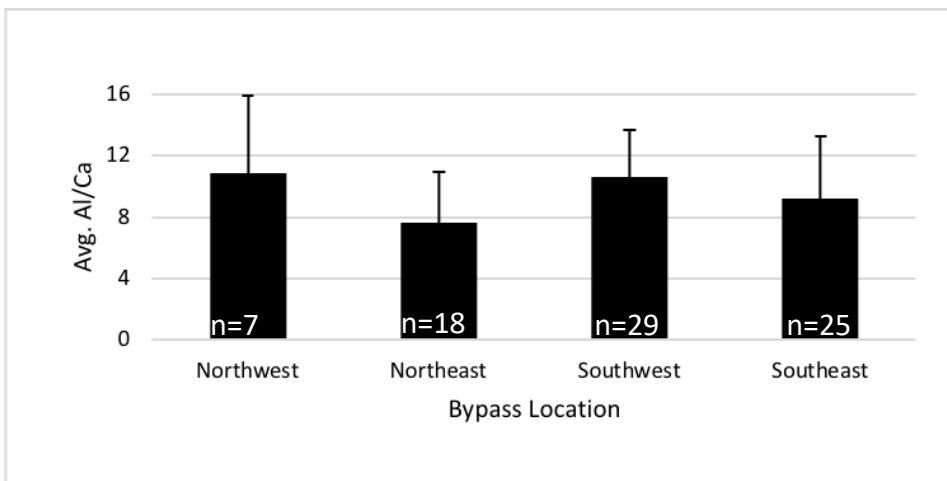
Figure 10. Average Al/Ca values for each quadrant.
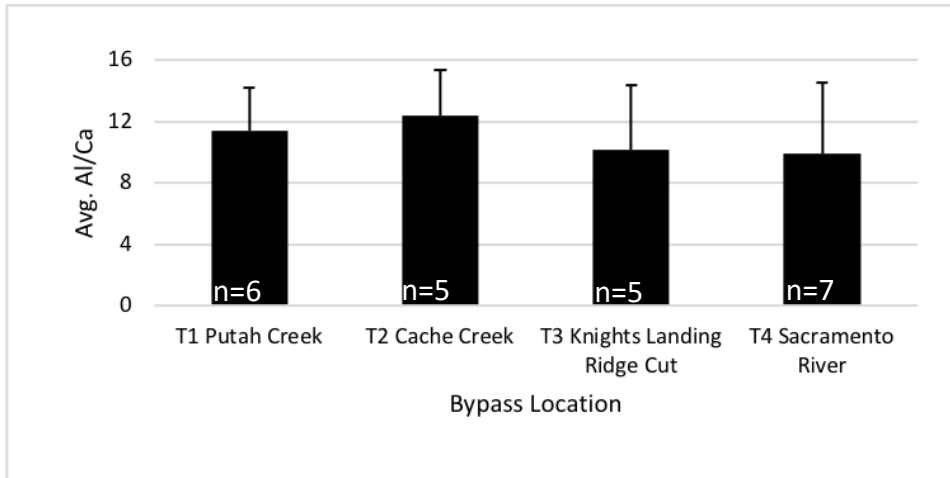
Figure 11. Average Al/Ca value for each transect core.
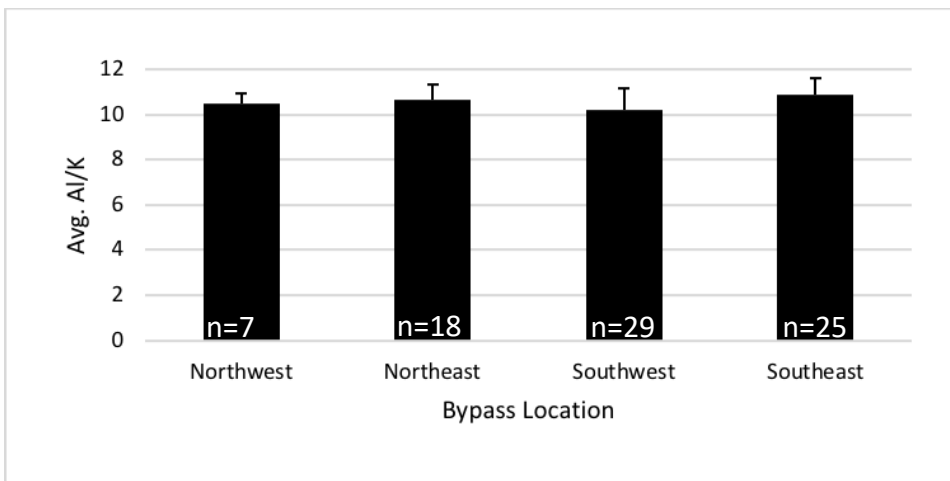
Figure 12. Average Al/K value for each quadrant.
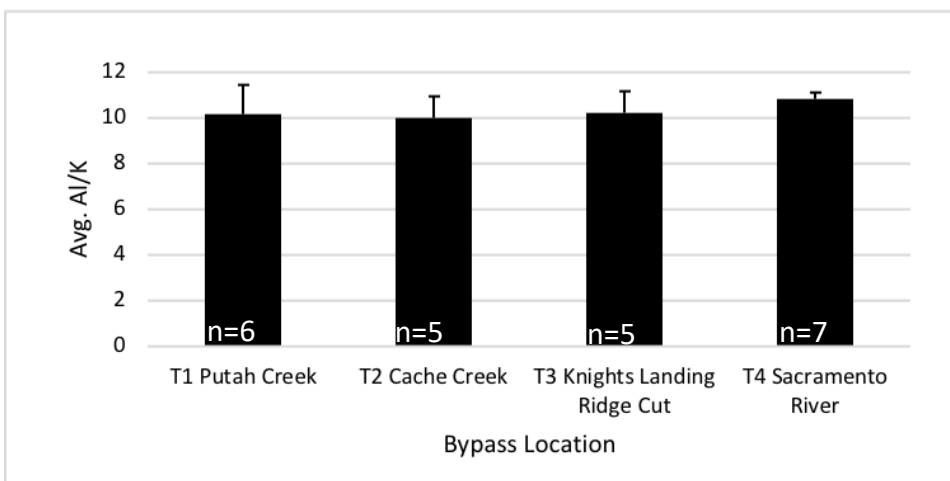
Figure 13. Average Al/K value for each transect core.
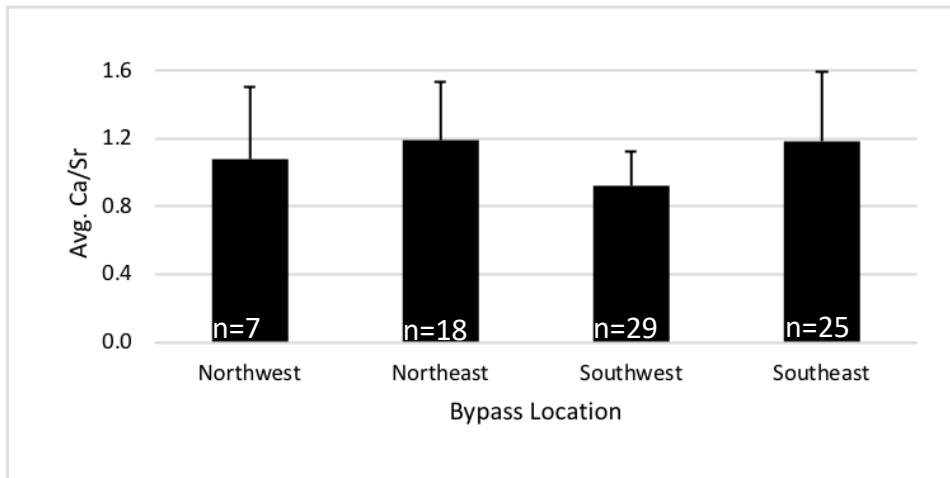
Figure 14. Average Ca/Sr value for each quadrant.
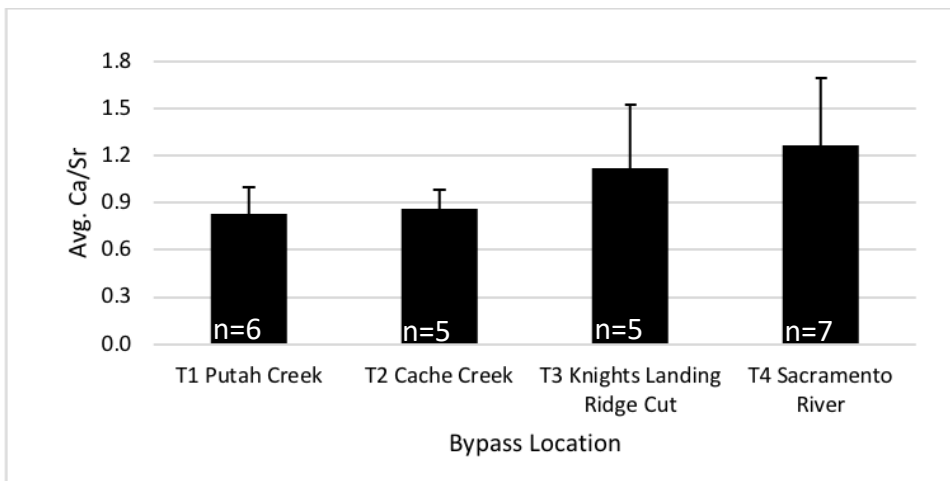
Figure 15. Average Ca/Sr value for each transect core.
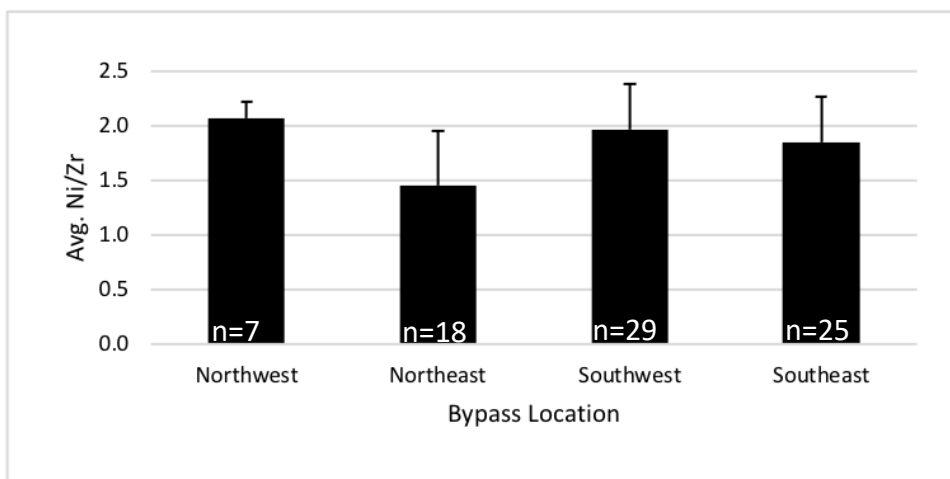
Figure 16. Average Ni/Zr value for each quadrant.
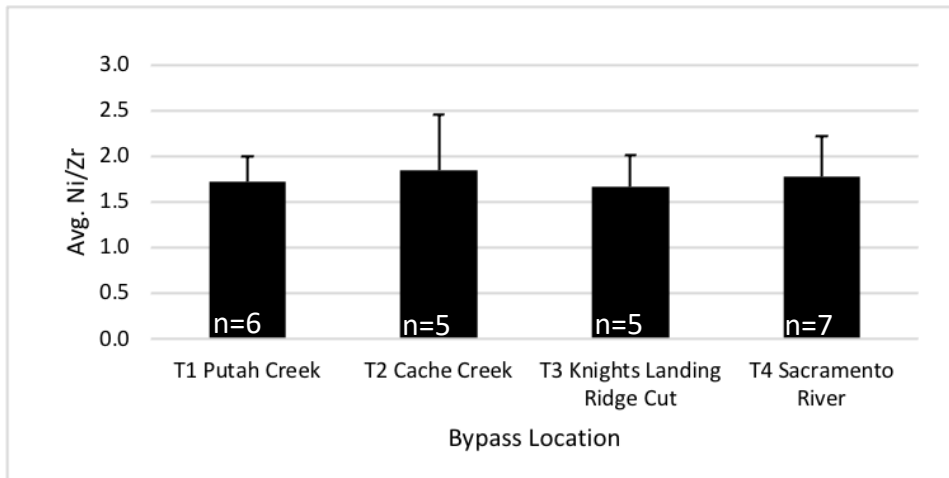
Figure 17. Average Ni/Zr value for each transect core.

Only one ANOVA test was performed for the Al/Ca and Ni/Zr values since there were no outliers, while two ANOVA tests were performed for Al/K and Ca/Sr since there were outliers present. The Al/Ca, Al/K, Ca/Sr, and Ni/Zr values from all core samples within the northwest, northeast, southwest, and southeast quadrants were used respectively for each ANOVA test. ANOVA tests revealed that differences in the means of Al/Ca, Al/K, Ca/Sr, and Ni/Zr varied significantly according to quadrant. T-tests also showed differences in these ratios between the bypass's western and eastern cores. The Indian Hill Tertiary *in-situ* upper- and lower-unit sample values for Al/Ca are 65 and 53, Al/K are 11 and 12, Ca/Sr are 0.6 and 0.7, and Ni/Zr are 1.0 and 0.8, respectively.

Mercury Concentrations

A total-mercury analysis was completed for all 84 samples (Table 3). Mercury concentrations in the core samples range from 0.03 ppm to 1.3 ppm with a LOD of 0.005 ppm (Actlabs, 2018). The average of all the Hg concentrations in the core samples is 0.15 ±

0.20 ppm. The highest Hg concentrations are in the core samples located on the southwest

side of the Yolo Bypass, where sediment is coming from Cache Creek and Putah Creek (Fig.

18). The lowest concentration of Hg is in the northeast quadrant of the bypass. The transect

core sample averages show that transect T2, where sediment is coming from Cache Creek,

contains the highest average concentration of Hg (Fig. 19). ANOVA tests revealed that

differences in the means of Hg concentrations varied significantly according to quadrant. A

T-test also showed differences in the means between Hg concentrations and the bypass's

western and eastern cores. The Indian Hill upper- and lower-unit *in-situ* samples have Hg

concentrations of 0.021 and 0.098 ppm, respectively.
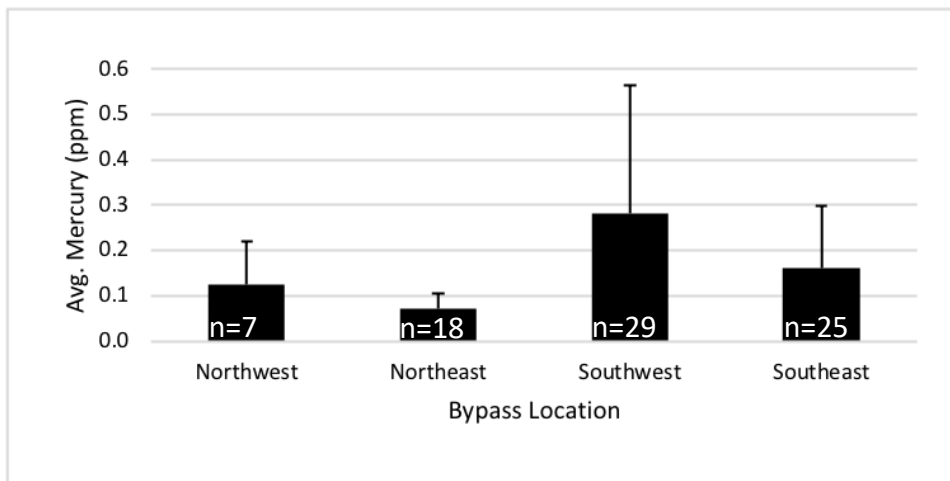
Figure 18. Average Hg concentration for each quadrant.

To determine if there was any relationship between Hg concentration and other

geochemical and mineralogical compositions, Hg was plotted against Pb, Fe_2O_3, Q/P, Al/Ca,

Al/K, Ca/Sr, and Ni/Zr for all the core samples. No significant relationships were found

between Hg and any of geochemical and mineralogical compositions when all samples in
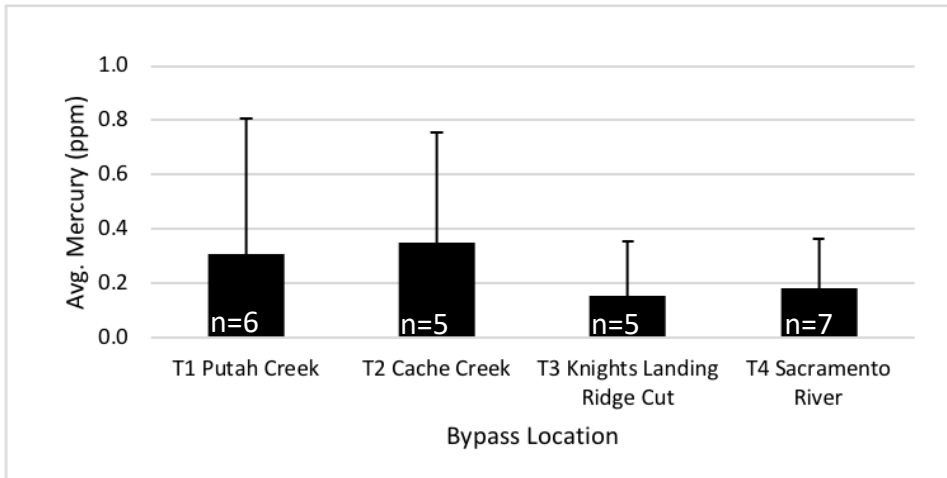
Figure 19. Average Hg concentration for each transect core.

the bypass were in the same plot. Next, to determine if there was any relationship between Hg concentration and geochemical and mineralogical compositions according to location in the bypass, Hg was plotted against Pb, Fe, quartz-to-plagioclase, Al/Ca, Al/K, Ca/Sr, and Ni/Zr for each of the quadrants. Mercury concentration plotted against Pb concentration in the northeast quadrant had a moderate relationship with an R^2 value of 0.44 (Fig. 20). There were no other significant relationships present in any of the quadrants.

Different chemical and mineralogical constituents were used, including Hg, Al/Ca, Ca/Sr, Ni/Zr, Q/P, and CaO, in determining if any sediment sample contained HMS. First, the Hg background concentrations from the pre-gold rush sediment needed to be established. This study and other studies have determined background Hg concentrations in surrounding areas (Table 5). The two Indian Hill *in-situ* Tertiary gravel samples from the upper- and lower- units were collected to represent the pre-mining Hg levels from the Sierra Nevada. The Hg levels for the upper unit had a concentration of 0.021 ppm and the lower unit was

measured at 0.098 ppm. The global average crustal abundance of Hg concentration is 0.067

ppm (Cox, 1989).
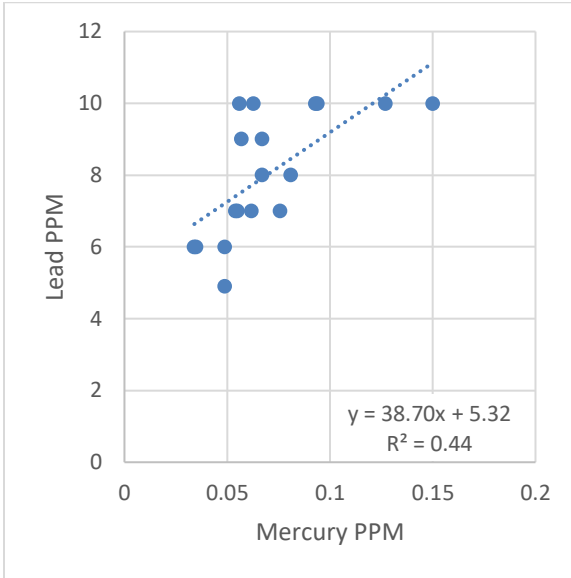
Figure 20. Northeast quadrant, lead concentrations plotted against mercury concentrations.

TABLE 5. BACKGROUND MERCURY CONCENTRATIONS

	[Hg] (ppm)			
Background	HMS	Post-mining	Study	Location
0.03-0.08	0.09-0.45	0.16-0.79	Bouse et al., 2010	San Francisco Bay
0.1-0.3	N.A.	N.A.	Domagalski et al., 2004	Cache Creek Watershed
0.04-0.05	N.A.	N.A.	James et al., 2009	Yuba and Feather Rivers
0.017-0.056	N.A.	N.A.	Nakamura et al., 2018	Blue Point Mine
0.021-0.098	N.A.	N.A.	This study	Indian Hill
0.01-0.051	N.A.	N.A.	This study	Blue Point Mine
0.034-0.193	0.076-0.122	0.049-0.508	This study	Yolo Bypass east quads.
0.067	N.A.	N.A.	Cox, 1989	Global average
N.A. = not applicable.				

   Using the background concentration values from this study and the other studies, a

background concentration of 0.075 ppm was used to distinguish HMS from pre-mining

sediment. All the cores had samples with Hg levels above the global average and above the

pre-mining levels. Based on Hg concentration alone, the HMS can be identified at specific

depths throughout the eastern quadrants of the bypass (Table 6). The depths in Table 6 are

the upper contact; above this, the sediment is classified as post-mining sediment. Only the

samples from the northeast and southeast quadrants were used since HMS comes from the

Sierra Nevada and is more prominent in the eastern bypass. Borehole C9 was not deep

enough to reach the pre-gold rush sediment and was omitted.

TABLE 6. UPPER CONTACT DEPTHS OF SEDIMENT CONTAINING HMS BASED ON
GEOCHEMICAL AND MINEROLOGICAL SIGNATURES

Borehole identifier	Depth of HMS based on proxies (cm)						Depth to HMS (cm)
	Hg	Al/Ca	Ni/Zr	Ca/Sr	CaO	Quartz/Plag	
TW1	218	218	307	218	218	218	218
C1	98	98	98	98	98	98	98
C5	206	206	138	206	206	206	206
C17	310	310	278	310	310	310	310
T3	102	102	191	102	102	102	102
T4	208	208	292	208	208	208	208

End-Member Mixing Analysis

An EMMA was only done for the core samples from the eastern quadrants since the

eastern quadrants contain significant amounts of HMS (Table 7). The two tracers used in the

EMMA were CaO percentages and the Ca/Sr values. The maximum fraction of HMS in the

eastern quadrants core samples is approximately 94%. These results presume that pre-

mining (modern) sediment and HMS, are the sole contributors of sediment in the eastern

quadrants of the bypass.

TABLE 7. EMMA SHOWING PERCENTAGE OF HMS IN THE CORE SAMPLES FOR THE EASTERN QUADRANTS IN THE YOLO BYPASS

Sample identifier	Depth (cm)	CaO (%)	Ca/Sr
TW1-A	20	72	63
TW1-B	116	70	64
TW1-C	208	81	71
TW1-D	218	83	76
TW1-E	307	63	50
TW1-F	409	68	54
T3-A	14	88	86
T3-B	102	89	91
T3-C	191	81	84
T3-D	290	51	30
T3-E	402	80	67
T4-A	15	86	77
T4-B	108	84	75
T4-C	159	86	77
T4-D	208	88	79
T4-E	292	69	56
T4-F	323	1	4
T4-G	399	77	68
C1-A	33	80	67
C1-B	98	85	73
C1-C	212	78	71
C1-D	269	76	69
C1-E	303	73	62
C1-F	406	69	64
C5-A	33	81	84
C5-B	100	84	87
C5-C	138	75	70
C5-D	206	88	94
C5-E	314	7	32
C5-F	409	59	64
C17-A	19	84	79
C17-B	105	64	62
C17-C	135	72	65
C17-D	215	87	91
C17-E	278	86	94
C17-F	310	82	93
C17-G	317	68	61
C17-H	329	11	1
C17-I	368	25	33

Mineralogy

Overall, the mineralogy of the core samples is similar throughout the bypass (Table 8).

The Q/P values in the core samples ranges from 1.0 to 2.2 (Table 9). The average Q/P value

in the core samples is 1.6 ± 0.26.

TABLE 8. MINERALS PRESENT IN SAMPLES FROM THE YOLO BYPASS, INDIAN HILL, AND BLUE POINT MINE

Sample identifier	Minerals identified from XRD							
TW1-A	Quartz	Clinochlore	N.D.	Albite	Muscovite	N.D.	N.D.	N.D.
TW1-B	Quartz	Clinochlore	N.D.	Albite	Muscovite	N.D.	N.D.	N.D.
TW1-C	Quartz	Clinochlore	N.D.	Albite	Muscovite	N.D.	N.D.	N.D.
TW1-D	Quartz	Clinochlore	N.D.	Albite	Muscovite	N.D.	N.D.	N.D.
TW1-E	Quartz	Clinochlore	N.D.	Albite	Muscovite	N.D.	N.D.	N.D.
TW1-F	Quartz	Clinochlore	N.D.	Albite	Muscovite	N.D.	N.D.	N.D.
C1-A	Quartz	Clinochlore	Vermiculite	Albite	Muscovite	N.D.	N.D.	Anorthite
C1-B	Quartz	N.D.	Vermiculite	N.D.	Muscovite	Chlorite	N.D.	Anorthite
C1-C	Quartz	N.D.	Vermiculite	Albite	Muscovite/Biotite	N.D.	N.D.	N.D.
C1-D	Quartz	Clinochlore	Vermiculite	Albite	N.D.	Chlorite	N.D.	N.D.
C1-E	Quartz	Clinochlore	Vermiculite	Albite	N.D.	Chlorite	Labradorite	N.D.
C1-F	Quartz	Clinochlore	Vermiculite	Albite	N.D.	Chlorite	N.D.	N.D.
C4-A	Quartz	Clinochlore	N.D.	Albite	N.D.	Chlorite	Labradorite	N.D.
C4-B	Quartz	Clinochlore	N.D.	Albite	N.D.	Chlorite	N.D.	N.D.
C4-C	Quartz	Clinochlore	N.D.	Albite	N.D.	Chlorite	N.D.	N.D.
C4-D	Quartz	Clinochlore	N.D.	Albite	Muscovite	N.D.	Labradorite	N.D.
C4-E	Quartz	Clinochlore	Vermiculite	Albite	Muscovite	N.D.	N.D.	N.D.
C4-F	Quartz	Clinochlore	N.D.	Albite	Muscovite	N.D.	Labradorite	N.D.
C4-G	Quartz	Clinochlore	N.D.	Albite	Muscovite	N.D.	Labradorite	N.D.
C5-A	Quartz	Clinochlore	N.D.	Albite	Muscovite	N.D.	N.D.	N.D.
C5-B	Quartz	Clinochlore	N.D.	Albite	Muscovite	N.D.	N.D.	N.D.
C5-C	Quartz	Clinochlore	Vermiculite	Albite	Muscovite	N.D.	N.D.	N.D.
C5-D	Quartz	Clinochlore	Vermiculite	Albite	N.D.	N.D.	Labradorite	N.D.
C5-E	Quartz	Clinochlore	N.D.	Albite	Muscovite	N.D.	N.D.	Dolomite
C5-F	Quartz	Clinochlore	N.D.	Albite	Muscovite	Chlorite	N.D.	N.D.

TABLE 8. (CONTINUED)

Sample identifier					Minerals identified from XRD			
C8-A	Quartz	Clinochlore	N.D.	Albite	Muscovite	Chlorite	N.D.	N.D.
C8-B	Quartz	Clinochlore	N.D.	Albite	N.D.	N.D.	N.D.	N.D.
C8-C	Quartz	Clinochlore	N.D.	Albite	N.D.	N.D.	N.D.	N.D.
C8-D	Quartz	Clinochlore	N.D.	Albite	N.D.	N.D.	N.D.	N.D.
C8-E	Quartz	Clinochlore	N.D.	Albite	N.D.	N.D.	N.D.	N.D.
C8-F	Quartz	Clinochlore	N.D.	Albite	N.D.	N.D.	N.D.	N.D.
C8-G	Quartz	Clinochlore	N.D.	Albite	N.D.	N.D.	N.D.	N.D.
C8-H	Quartz	Clinochlore	N.D.	Albite	N.D.	N.D.	N.D.	N.D.
C8-I	Quartz	Clinochlore	N.D.	Albite	N.D.	N.D.	N.D.	N.D.
C8-J	Quartz	Clinochlore	N.D.	Albite	N.D.	N.D.	N.D.	N.D.
C9-A	Quartz	Clinochlore	N.D.	Albite	Muscovite	N.D.	N.D.	N.D.
C9-B	Quartz	Clinochlore	N.D.	Albite	Muscovite	N.D.	N.D.	N.D.
C9-C	Quartz	Clinochlore	N.D.	Albite	Muscovite	N.D.	N.D.	N.D.
C9-D	Quartz	Clinochlore	N.D.	Albite	N.D.	N.D.	N.D.	N.D.
T1-A	Quartz	Clinochlore	N.D.	Albite	Muscovite/Biotite	N.D.	N.D.	N.D.
T1-B	Quartz	Clinochlore	N.D.	Albite	Muscovite	N.D.	N.D.	N.D.
T1-C	Quartz	Clinochlore	N.D.	Albite	N.D.	N.D.	N.D.	N.D.
T1-D	Quartz	Clinochlore	N.D.	Albite	Muscovite	N.D.	N.D.	N.D.
T1-E	Quartz	Clinochlore	N.D.	Albite	Muscovite	N.D.	N.D.	N.D.
T1-F	Quartz	Clinochlore	N.D.	Albite	Muscovite	N.D.	N.D.	N.D.
T2-A	Quartz	Clinochlore	N.D.	Albite	Muscovite	N.D.	N.D.	N.D.
T2-B	Quartz	Clinochlore	N.D.	Albite	Muscovite	N.D.	N.D.	N.D.
T2-C	Quartz	Clinochlore	N.D.	Albite	Muscovite	N.D.	N.D.	N.D.
T2-D	Quartz	Clinochlore	N.D.	Albite	Muscovite	N.D.	N.D.	N.D.
T2-E	Quartz	Clinochlore	N.D.	Albite	Muscovite	N.D.	N.D.	N.D.
T3-A	Quartz	Clinochlore	N.D.	Albite	Muscovite	N.D.	N.D.	N.D.
T3-B	Quartz	Clinochlore	N.D.	Albite	Muscovite	N.D.	N.D.	N.D.
T3-C	Quartz	Clinochlore	N.D.	Albite	Muscovite	N.D.	N.D.	N.D.
T3-D	Quartz	Clinochlore	N.D.	Albite	Muscovite	N.D.	N.D.	N.D.
T3-E	Quartz	Clinochlore	N.D.	Albite	Muscovite	N.D.	N.D.	N.D.
T4-A	Quartz	Clinochlore	N.D.	Albite	Muscovite	N.D.	N.D.	N.D.
T4-B	Quartz	Clinochlore	N.D.	Albite	Muscovite	N.D.	N.D.	N.D.
T4-C	Quartz	Clinochlore	N.D.	Albite	Muscovite	N.D.	N.D.	N.D.
T4-D	Quartz	Clinochlore	N.D.	Albite	Muscovite	N.D.	N.D.	N.D.
T4-E	Quartz	Clinochlore	N.D.	Albite	Muscovite	N.D.	N.D.	N.D.
T4-F	Quartz	Clinochlore	N.D.	Albite	Muscovite	N.D.	N.D.	N.D.
T4-G	Quartz	Clinochlore	N.D.	Albite	Muscovite	N.D.	N.D.	N.D.

TABLE 8. (CONTINUED)

Sample id.	Minerals identified from XRD							
C16-A	Quartz	Clinochlore	N.D.	Albite	N.D.	N.D.	N.D.	N.D.
C16-B	Quartz	N.D.	Vermiculite	N.D.	N.D.	N.D.	N.D.	N.D.
C16-C	Quartz	Clinochlore	N.D.	Albite	N.D.	Chlorite	N.D.	Dolomite
C16-D	Quartz	Clinochlore	Vermiculite	Albite	N.D.	N.D.	N.D.	N.D.
C16-E	Quartz	Clinochlore	N.D.	Albite	N.D.	N.D.	N.D.	N.D.
C16-F	Quartz	N.D.	Vermiculite	Albite	N.D.	N.D.	N.D.	N.D.
C16-G	Quartz	Clinochlore	N.D.	Albite	Muscovite	N.D.	N.D.	N.D.
C16-H	Quartz	Clinochlore	Vermiculite	Albite	N.D.	Chlorite	N.D.	N.D.
C17-A	Quartz	Clinochlore	N.D.	Albite	Muscovite	N.D.	N.D.	N.D.
C17-B	Quartz	Clinochlore	N.D.	Albite	N.D.	Chlorite	N.D.	N.D.
C17-C	Quartz	Clinochlore	Vermiculite	Albite	N.D.	Chlorite	N.D.	N.D.
C17-D	Quartz	Clinochlore	Vermiculite	Albite	N.D.	N.D.	N.D.	N.D.
C17-E	Quartz	Clinochlore	Vermiculite	Albite	N.D.	N.D.	N.D.	N.D.
C17-F	Quartz	Clinochlore	Vermiculite	Albite	Muscovite	N.D.	N.D.	N.D.
C17-G	Quartz	Clinochlore	Vermiculite	Albite	N.D.	N.D.	N.D.	N.D.
C17-H	Quartz	Clinochlore	Vermiculite	Albite	N.D.	N.D.	N.D.	N.D.
C17-I	Quartz	Clinochlore	N.D.	Albite	Muscovite	N.D.	Labradorite	N.D.
IH_Tg Upper	Quartz	Clinochlore	N.D.	N.D.	Muscovite/Biotite	N.D.	N.D.	Kaolinite
IH_Tg Lower	Quartz	Clinochlore	N.D.	N.D.	Muscovite/Biotite	N.D.	N.D.	Kaolinite
M1 (BPM)	Quartz	Clinochlore	N.D.	Albite	N.D.	N.D.	Labradorite	Kaolinite
M2S (BPM)	Quartz	Clinochlore	N.D.	Albite	N.D.	N.D.	Labradorite	Kaolinite
M3S (BPM)	Quartz	Clinochlore	N.D.	Albite	N.D.	N.D.	N.D.	Kaolinite

N.D. = not determined and/or identified from XRD analysis

TABLE 9. QUARTZ-TO-PLAGIOCLASE VALUES

Sample identifier	Depth (cm)	Quartz/Plag	Sample identifier	Depth (cm)	Quartz/Plag
TWI-A	20.0	1.12	T2-A	26.0	1.75
TWI-B	116.0	1.02	T2-B	104.0	1.53
TWI-C	208.0	1.29	T2-C	201.0	1.59
TWI-D	218.0	1.42	T2-D	250.0	1.84
TWI-E	307.0	1.24	T2-E	300.0	1.37
TWI-F	409.0	1.22	T3-A	14.0	1.77
C1-A	33.0	1.12	T3-B	102.0	1.98
C1-B	98.0	1.27	T3-C	191.0	1.67
C1-C	212.0	1.16	T3-D	290.0	1.37
C1-D	269.5	1.36	T3-E	402.0	1.51
C1-E	303.5	1.30	T4-A	15.0	1.70
C1-F	406.0	1.30	T4-B	108.0	1.57
C4-A	24.0	1.43	T4-C	159.0	1.71
C4-B	100.5	1.55	T4-D	208.0	1.56
C4-C	203.0	1.42	T4-E	292.0	1.85
C4-D	311.0	1.75	T4-F	323.0	1.23
C4-E	356.0	1.94	T4-G	399.0	1.40
C4-F	402.5	1.62	C16-A	22.5	1.61
C4-G	495.0	1.37	C16-B	77.5	1.38
C5-A	33.0	1.78	C16-C	108.5	1.76
C5-B	100.0	1.67	C16-D	171.0	1.73
C5-C	138.0	1.63	C16-E	204.5	2.00
C5-D	206.0	1.84	C16-F	302.5	1.72
C5-E	314.0	1.52	C16-G	399.0	1.98
C5-F	409.0	1.48	C16-H	504.0	1.25
C8-A	30.0	1.60	C17-A	19.0	1.69
C8-B	102.0	1.29	C17-B	105.0	1.73
C8-C	174.0	1.90	C17-C	135.0	1.60
C8-D	199.0	1.81	C17-D	215.0	1.89
C8-E	214.0	1.99	C17-E	278.0	1.84
C8-F	308.5	1.58	C17-F	310.0	2.05
C8-G	382.0	2.09	C17-G	317.0	1.47
C8-H	405.0	1.61	C17-H	329.5	1.29
C8-I	457.0	2.08	C17-I	368.0	1.20
C8-J	490.0	1.42	IH_Tg Upper	N.A.	122.17
C9-A	36.0	1.92	IH_Tg Lower	N.A.	45.44
C9-B	57.0	1.75	M1(BPM)	N.A.	3.48
C9-C	120.0	1.68	M2S (BPM)	N.A.	15.13
C9-D	139.0	1.42	M3S (BPM)	N.A.	7.70
T1-A	20.0	1.57			
T1-B	107.0	2.18			
T1-C	138.0	1.80			
T1-D	208.0	1.55			
T1-E	302.0	1.61			
T1-F	373.0	1.50			

N.A. = not applicable.

The southwest quadrant has the highest average Q/P values (Fig. 21). The transect core

T1 has the highest average Q/P values compared to the rest of the transect cores (Fig. 22).

The ANOVA test revealed that differences in the means of Q/P varied significantly according

to quadrant. A T-test also showed differences in the means between Q/P and the bypass's

western and eastern cores. The Indian Hill Tertiary *in-situ* upper- and lower-unit samples

have Q/P values of 122 and 45, respectively.
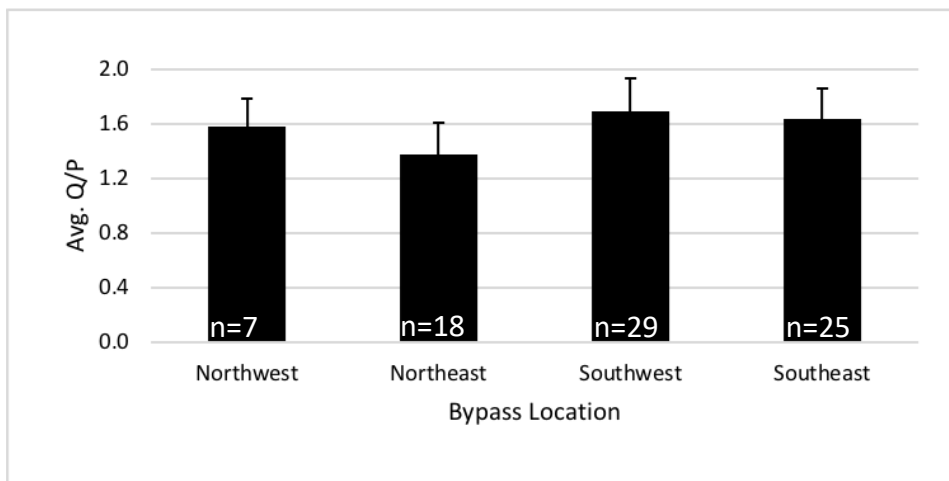
Figure 21. Average quartz-to-plagioclase values for each quadrant.
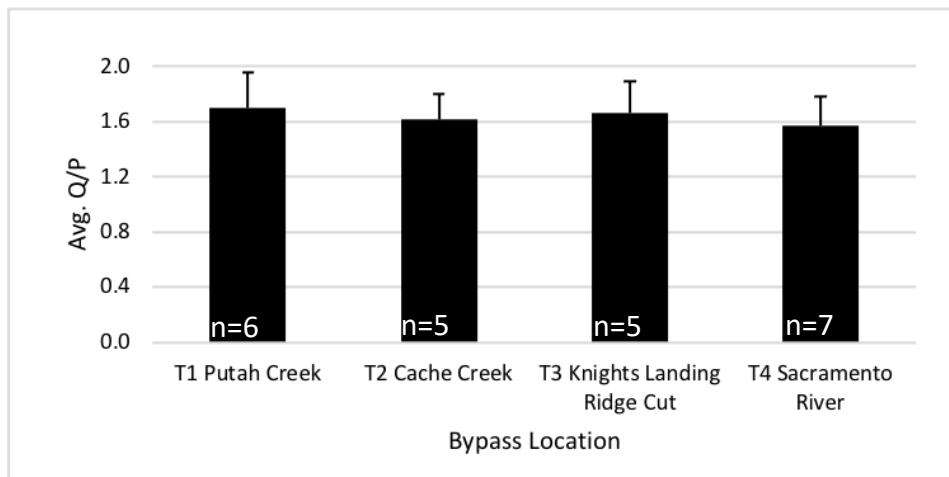
Figure 22. Average quartz-to-plagioclase values for each transect core.

The clay compositions were analyzed for the transect core samples T1A, T1C, T2A, T3D, T4B, and T4G. The six samples were selected specifically for their high and low Hg concentrations. Transect cores T1C, T3D, and T4G have low concentrations of Hg, whereas T1A, T2A, and T4B have high concentrations of Hg. All six samples contained expandable clays, shown by the glycolated peak shift (Figs. 3 and 4). The clays present are smectite, kaolinite, chlorite, and illite (Table 10, Figs. 3 and 4). Core samples T1A, T2A, and T4B have no chlorite present, whereas T1C, T3D, and T4G have chlorite present. All clay fractions contain smectite and kaolinite, highly expandable clays, whereas only some contain chlorite, a non-expansive clay (Barton, 2002). Interestingly the core samples high in Hg concentration had no chlorite present whereas samples low in Hg concentration had chlorite present. Based on the clay analysis there may exist an inverse relationship between Hg concentrations and chlorite.

TABLE 10. CLAYS PRESENT IN SELECTED TRANSECT SAMPLES (PERS. COMM. BRISTOW, 2018)

Sample identifier	Hg (ppm)					
T1-A	1.320	Smectite	Kaolinite	N.I.	N.I.	N.I.
T1-C	0.060	Smectite	Kaolinite	Chlorite	N.I.	< 10% mixed layers
T2-A	1.060	Smectite 90%	Kaolinite	N.I.	N.I.	< 10% mixed layers
T3-D	0.047	Smectite	Kaolinite	Chlorite	Illite	< 10% mixed layers
T4-B	0.508	Smectite	Kaolinite	N.I.	Illite	N.I.
T4-G	0.040	Smectite	Kaolinite	Chlorite	Illite	< 10% mixed layers

N.I. = no other clays identified.

DISCUSSION

Geochemical and Mineralogical Signatures of HMS

Eastern and Western Quadrants

A concise summary of geochemical and mineralogical findings in the bypass is as follows. The western quadrants of the bypass, the side receiving sediment from the Coast Ranges, have higher averages of Hg concentrations, Al/Ca, Ni/Zr, and Q/P values compared to the eastern quadrants. The eastern quadrants of the bypass, which receive sediment from the Sierra Nevada, have higher averages of CaO percentages, Ca/Sr, and Al/K values compared to the western quadrants. The pre-mining sediment has lower Hg concentrations, Al/Ca values, and Q/P values, in addition to higher CaO percentages, Ca/Sr, and Ni/Zr values when compared to HMS. The samples containing HMS have higher Hg concentrations, Al/Ca values, and Q/P values, in addition to lower CaO percentages, Ca/Sr values, and Ni/Zr values compared to modern sediment.

The first goal of this study was to determine if there is a distinguishable geochemical and mineralogical signature for sediment containing HMS within the bypass. The first step was to identify geochemical differences in the sediment coming from the Coast Ranges versus the Sierra Nevada. There are significant chemical and mineralogical differences in the sediment in the eastern versus the western quadrants of the bypass when comparing Hg concentrations, Al/Ca, Al/K, Ni/Zr, Q/P, Ca/Sr values, and CaO percentages (Figs. 11, 13, 15, 17, 19, and 22; Tables 3, 4, and 9).

Mercury concentrations are higher in the sediment coming from the Coast Ranges (Fig.

19). The western quadrants of the bypass have an average Hg concentration of 0.19 ± 0.26

ppm, whereas the eastern quadrants have an average Hg concentration of 0.12 ± 0.12 ppm.

The Coast Ranges sediment brings in more Hg from cinnabar mining than the HMS from

historic gold mining in the Sierras (Springborn et al., 2011). Cache Creek alone brings in 64%

of Hg into the bypass (Springborn et al., 2011).

Mercury concentrations are the highest in the southern quadrants of the bypass, with

the southwest quadrant having the highest concentrations (Fig. 18). One potential reason

that Hg concentrations are higher in the southern quadrants of the bypass is that Hg has a

higher adsorption to clay's greater surface area (Kongchum et al., 2011). A companion study

found higher amounts of fine sediment (< 63 μm) in the southern portions of the bypass

(Mykytyn, personal communication, 2021). In addition, mercury concentrations are highest

in the top 50 cm of sediment in most of the bypass cores (Table 3; Appendix 2). The higher

Hg concentrations near the top of the cores can be attributed to Hg-mining in the Coast

Ranges and hydraulic mining in the Sierra Nevada. Keeping track of Hg concentrations in the

bypass is of great importance due to the negative environmental and biological impacts Hg

has on ecosystems (Wiener et al., 2007). The greatest focus on Hg concentrations, by those

intending to remediate the bypass, should be in the southwest quadrant of the bypass.

The hydraulically mined upper-auriferous gravels primarily consist of quartz clasts

(Lindgren, 1911; Yeend, 1974). Thus, sediment derived from HMS should have high quartz

content (James, 1991; Bouse et al., 2010). An assumption made in this study was that the

eastern quadrants were likely to have a higher Q/P value than the western quadrants, since

HMS should have high quartz content compared to pre-mining sediment (Bouse et al.,

2010). Unexpectedly, the Q/P values were similar throughout the bypass. The average Q/P

value for the western quadrants is 1.6 ± 0.4 while the average value for the eastern

quadrants is 1.5 ± 0.4. A possible reason for the similar values across the bypass could be

that Hg mined sediment, coming from the Coast Ranges, is also high in quartz due to Hg

being mined in a silica rich environment (Studemeister, 1984). A future study could get *in-*

situ samples from the Coast Ranges as well as some samples from the cinnabar mines near

the Cache creek watershed for comparison.

The Al/Ca and Al/K ratios are often used as indicators of the intensity of weathering

(Wei et al., 2006; Yang and Du, 2017). The auriferous gravels underwent intense weathering

during the Eocene therefore sediment derived from the gravels should have higher Al/Ca

and Al/K values compared to modern sediment (Chapin III et al., 2011; Cassel et al., 2012).

The Al/Ca average value for the western quadrants is 10.4 ± 3.8 while the average value for

the eastern quadrant is 8.4 ± 3.8, a t-test was performed, and these values are statistically

significant. The differences between Al/Ca values in the eastern and western quadrants

might be due to more intense chemical weathering in the Coast Ranges as Ca is leached at

higher rates than Al during chemical weathering (Nesbitt and Young, 1982). Another cause

for the differences could be that cinnabar mining sediment from the Coast Ranges lacks

calcic material when compared to plagioclase (Barnes et al., 1973; Bouse et al., 2010). The

Al/K values are similar between the eastern and western quadrants. The average Al/K value

for the eastern quadrants is 10.8 ± 0.7 while the average Al/K for the western quadrants is

10 ± 1.9. These values would indicate that the sediment in the bypass have undergone

similar weathering histories since high Al/K values indicate intense chemical weathering.

Goldhaber et al. (2009) found that sediment on the eastern portion of the Sacramento

floodplain has a higher Ca/Sr relative to sediment on the western portion of the Sacramento

floodplain. A similar trend is present in the bypass with the eastern quadrants having a

higher average Ca/Sr value of 1.2 ± 0.4, whereas the western quadrants average value is 0.9

± 0.3. Trending similarly with Ca/Sr, the CaO average for the eastern quadrants of the

bypass is 1.81 ± 0.6 and for the western quadrants is 1.36 ± 0.4. A T-Test was performed on

the Ca/Sr and CaO average values and the means variances were significant. The differences

are likely caused by a lack of calcic material in the cinnabar mining sediment from the Coast

Ranges compared to the Sierra Nevada which is high in granitic rocks which are enriched in

plagioclase and amphibole, two important carriers of Ca and Sr (Turner, 1899; Barnes et al.,

1973; Probst et al., 2000; Bouse et al., 2010).

Nickel concentrations are higher in the western Sacramento Valley compared to the

eastern Sacramento Valley and a similar trend is present in the bypass (Goldhaber et al.,

2009). The western quadrants of the bypass have a Ni/Zr average of 1.93 ± 0.5, whereas the

eastern quadrants of the bypass have a Ni/Zr average of 1.6 ± 0.5. The differences are likely

caused by sediment being derived from the Coast Range Ophiolite which are high in Ni

whereas the sediment being derived from the Sierra Nevada is primarily from granitic

sources. Since the western and eastern quadrants have significant chemical and

mineralogical differences, only the eastern quadrants bypass core samples were used to quantify fractions of HMS.

Hydraulic Mining Sediment

The auriferous gravels were deposited during the Eocene, which had a warm and wet climate (Allen, 1929; Cassel and Graham, 2011; Mix et al., 2015). Since the granitic clasts underwent intense chemical weathering, higher concentrations of Al, lower concentrations of Ca, and higher Q/P values were expected in the *in-situ* samples compared to modern sediment (Wei et al., 2006; Yang and Du, 2017). The Indian Hill upper-and lower- unit *in-situ* samples had Al/Ca values of 64 and 53, respectively. These are high values compared to modern sediment and sediment in the bypass. The fractions of sediment in the bypass that contain HMS will therefore have higher Al/Ca values than the modern sediment. This study found pre-, contemporaneous, and post-mining Al/Ca values of 1.78-8.59, 9.41-14.38, and 5.16-13.92, respectively, in the sediment samples (Table 11). Another set of Al/Ca background values, used in determining HMS, was from Bouse et al. (2010) (Table 11). Bouse et al. (2010) have Al/Ca values for pre-, contemporaneous, and post-mining sediment of 2.1-7.1, 7.8-18.9, and 5.0-8.5, respectively. Based on these Al/Ca values, the HMS can be identified at certain depths throughout the bypass (Table 6).

The other constituents that were analyzed were the Ca/Sr ratio and CaO percentages. The Indian Hill *in-situ* upper-and lower-unit samples have Ca/Sr values of 0.63 and 0.71, and CaO values of 0.22 and 0.29, respectively (Table 11). The Indian Hill values were significantly lower than the borehole core samples from the bypass. Bouse et al. (2010) showed that

TABLE 11. PRE-, CONTEMPORANEOUS, POST- MINING VALUES

Indices	Background	HMS	Post-mining	Study	Location
Al/Ca	2.1-7.1	7.8-18.9	5-8.5	Bouse et al., 2010	San Francisco Bay
Al/Ca	1.78-8.59	9.41-14.38	5.16-13.92	This Study	Yolo Bypass east. quad.
Al/Ca	52.97-64.64	N.A.	N.A.	This Study	Indian Hill
Ni/Zr	1.11-1.30	0.77-1.15	1.24-1.76	Bouse et al., 2010	San Francisco Bay
Ni/Zr	0.81-0.98	N.A.	N.A.	This Study	Indian Hill
Ca/Sr	1.13-2.26	0.76-1.10	0.76-1.26	This Study	Yolo Bypass east. quad.
Ca/Sr	0.63-0.71	N.A.	N.A.	This Study	Indian Hill
CaO (%)	1.64-7.31	1.04-1.50	1.1-2.79	This Study	Yolo Bypass east. quad.
CaO (%)	0.22-0.29	N.A.	N.A.	This Study	Indian Hill
Quartz/Plag	1.16-1.85	1.27-2.05	1.02-1.78	This Study	Yolo Bypass east. quad.
Quartz/Plag	45.44-122.17	N.A.	N.A.	This Study	Indian Hill

N.A. = not applicable.

HMS should have lower Ca/Sr values and CaO percentages whereas pre-mining sediment should have the highest Ca/Sr values. The Ca/Sr values determined in this study for pre-, contemporaneous, post-mining sediments, are 1.13-2.26, 0.76-1.10, and 0.76-1.26, respectively. The CaO percentages determined by this study, for pre-, contemporaneous, post-mining, are 1.64-7.31, 1.04-1.50, and 1.1-2.79, respectively. By comparing Ca/Sr values, CaO percentages, and Al/Ca values, the HMS can be identified at certain depths throughout the bypass (e.g., Fig. 23).

The *in-situ* Indian Hill samples had lower Ni/Zr values of 0.98 for the upper unit and 0.81 for the lower unit, when compared to the bypass samples. Based on the study by Bouse et al. (2010), HMS should have lower values of Ni/Zr than the pre-mining sediment, although this was not the case for most core samples in the eastern quadrants of the bypass. I assumed that since the Indian Hill samples had low Ni/Zr, the HMS would have lower Ni/Zr values than the pre-mining sediment but that was not the case for every core sample in the
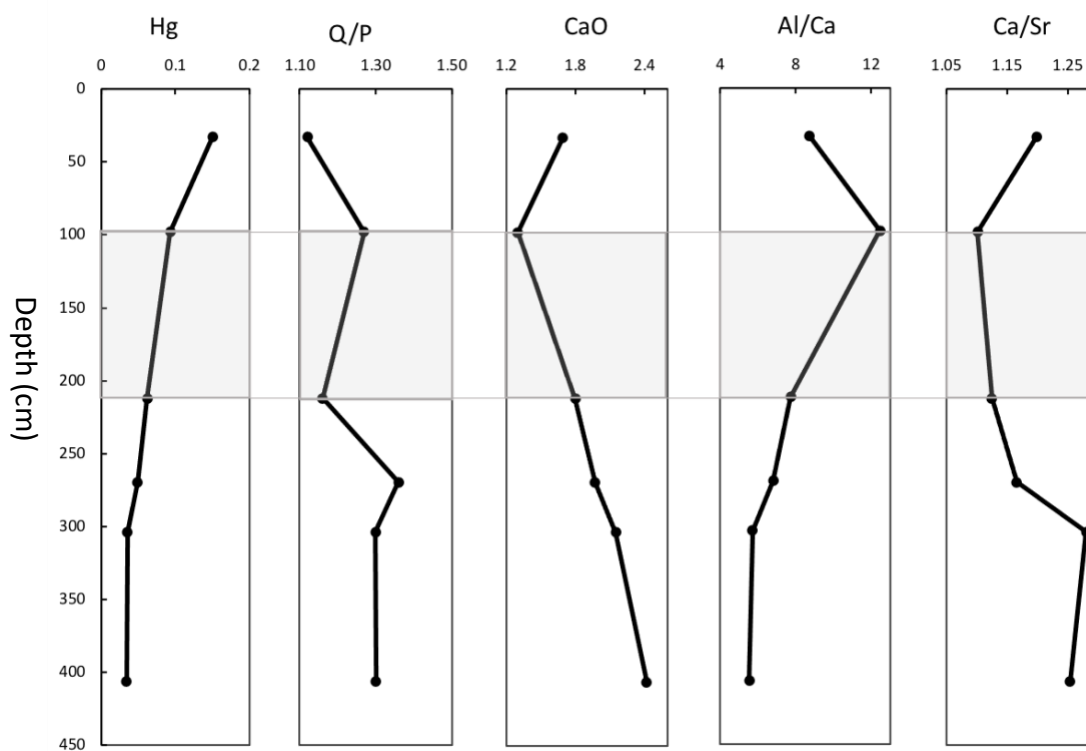
Figure 23. Depth profiles of borehole core C1. The shaded region is where HMS is noticeably present.

eastern quadrants of the bypass. Although the eastern quadrants did have a lower Ni/Zr compared to the western quadrants, the Ni/Zr values were not useful in determining the transition from pre-mining sediment to HMS as the Ni/Zr values were too variable between samples. Therefore, HMS and post-mining Ni/Zr values could not be defined and Bouse et al. (2010) pre-, contemporaneous, and post-mining values were used as guidance (Table 11). Therefore, Ni/Zr was ineffective in the classification of sediment as HMS and was only used in identifying sediment from the Coast Ranges or the Sierra Nevada. A possible reason for the varied Ni/Zr values between samples could be that there are other sediment sources from the Sierra Nevada that bring in Ni into the bypass, such as the western metamorphic

belt (Morrison et al., 2009). Another possibility is that, while very little mixing occurs throughout the bypass, there may just be enough mixing to mask any fingerprint Ni/Zr could provide.

James (1991) determined that quartz concentrations could be used to classify sediment as HMS. The last index used in determining fractions of sediment as HMS is the Q/P ratio. The upper and lower units of the auriferous gravels contain an abundance of quartz and quartzite (Lindgren, 1911; Yeend, 1974). The Tertiary *in-situ* Indian Hill upper-and lower-unit samples have high Q/P values of 122 and 45, respectively, therefore sediment deposited in the bypass from hydraulic mining is likely to have high Q/P values when compared to pre- and post-mining sediment. This study determined the pre-, contemporaneous, post-mining Q/P values of 1.16-1.85, 1.27-2.05, and 1.02-1.78, respectively (Table 11). Therefore, the Q/P ratio was useful in determining the boundary between pre-mining sediment and HMS in most of the core samples from the eastern quadrants.

The EMMA results showed that there was at least 83% to 94% of HMS in approximately a meter of sediment in the borehole cores in the eastern quadrants (Table 7). Since there are significant amounts of HMS, it is vital to have a detailed geochemical and mineralogical fingerprint of the sediment in the bypass to properly maintain the bypass.

Mercury Relationships Between the HMS Signatures

The second goal of this study was to determine a relationship between Hg and the geochemical and mineralogical fingerprint of HMS. Unexpectedly there were no significant relationships between the geochemical indices and Hg concentrations throughout the

entire bypass. To be more thorough, Hg concentration was plotted against each geochemical index again, but according to quadrant. The results did not improve. In the northeast quadrant, Hg concentration had a moderate to weak relationship with Pb with an R^2 value of 0.44; beyond this relationship there were no other significant relationships between Hg concentrations and the geochemical indices. A strong relationship between Hg and the Q/P ratio was anticipated due to the high quartz concentrations throughout the auriferous gravels. Unexpectedly, there were no strong relationships between Hg and the Q/P ratio. A lack of relationship between Hg and the other geochemical indices may be due to a few factors. Mercury has an affinity for clays which may play a role in the lack of relationship as the Hg is unevenly distributed with high concentrations located in the southwest quadrant of the bypass (McLean and Bledsoe, 1992). Another factor could be subtle mixing of sediment coming into the bypass from the Coast Ranges and the Sierra Nevada. If high concentrations of Hg are the primary fingerprint of HMS, then the lack of relationships to other chemical and mineralogical indices means those indices are not as useful in determining HMS on their own.

Hydraulic Banding in the Yolo Bypass

The third goal was to determine if hydraulic banding leaves a geochemical signature in the sediment. There were significant differences between each band regarding the geochemical and mineralogical signatures produced by Hg, Pb, Fe_2O_3, Al/Ca, Al/K, Ca/Sr, Ni/Zr, and Q/P. The band flowing in from Cache Creek (T2) contains the highest concentrations of Hg, followed by the Putah Creek band (T1) (Fig. 19). Mercury

55

concentrations differ significantly between the two western and two eastern bands.

Sediment being brought in from Cache Creek (T2) have the highest concentrations of Hg,

whereas sediment coming from Knights Landing Ridge Cut (T3) have the lowest Hg

concentrations. Cache Creek (T2) band has the highest Hg concentrations because its

watershed hosted three mercury mining districts (Domagalski et al., 2004). Some mitigation

and monitoring efforts that have already been put in place are the Cache Creek Settling

Basin, constant monitoring from the USGS gage near Yolo County, and biannual Hg

monitoring by the Yolo County (US Army Corps of Engineers, 2003; Office of Emergency

Services, 2018). While the Cache Creek Settling Basin was engineered to curtail the

sediment loads and high Hg concentrations from the Yolo Bypass, Hg is still reaching the

bypass in high concentrations. Approximately 93% of the total sediment load passing the

Yolo gauge, which is near the start of Cache Creek in the Yolo County, is suspended

sediment, with 86% of the suspended sediment being silt and clay (US Army Corps of

Engineers, 2003). Hg concentrations are likely high when coming into the bypass since Hg

has an affinity for clays (McLean and Bledsoe, 1992). To control Hg within the bypass, the

sediment in the southwest quadrant and the sediment coming from Cache Creek (T2)

should be regularly monitored and there should be a remediation plan in place for the

entire bypass. Interestingly, solely analyzing the Hg concentrations in each band shows how

little mixing occurs between them.

Lead concentrations and Fe_2O_3 percentages are the highest in the Sacramento River

band (T4) (Figs. 7 and 9). The high Pb concentrations in the Sacramento band likely have

anthropogenic origins, such as urbanization, gasoline additives, and Pb in paint (Solt et al., 2015). The higher Fe_2O_3 percentages in the Sacramento River band (T4) are likely from drainage of inactive mines in the Iron Mountain in Northern California (Alpers et al., 2000). When the mine was active, runoff was directed to Spring Creek, which is a tributary to the Sacramento River (Alpers et al., 2000).

The Cache Creek band (T2) has the highest Al/Ca and Ni/Zr values (Figs. 11 and 17). The Ni/Zr values are higher in the western bands compared to the eastern bands due to sediment dilution from granitic sources in the Sierra Nevada (Morrison et al., 2009). The Ca/Sr value decreases from the western most band to the eastern most band, with the Sacramento River band (T4) having the highest Al/K and Ca/Sr values (Figs. 13 and 15).

Although I expected that the Q/P ratio would be the highest in the Sacramento River band (T4), this was not the case. The Putah Creek band (T1) has the highest Q/P value while the Sacrament River band (T4) has the lowest Q/P value (Fig. 22). The reason for the Q/P differences between the bands is likely due to cinnabar being mined in a silica-rich environment in the Coast Ranges (Studemeister, 1984). The sediment produced from mining cinnabar was and still is being transported from the Cache Creek watershed to the bypass. The sediment being high in silica or quartz and low in plagioclase likely caused the Q/P ratio to be higher in the western quadrants of the bypass.

There are definite differences between each band, making distinguishing between the bands straightforward. The distinct chemical signatures discovered means that there was little lateral mixing between the bands (Sommer et al., 2008). The little to no mixing is

caused by shallow flow depths (Sommer et al., 2008). The little to no mixing between the

hydrologic bands makes identifying hotspots for Hg or other pollutants less complex.

CONCLUSION

Hydraulic gold mining in the Sierra Nevada began in 1852, after which large amounts of hydraulic mining sediment (HMS) was transported to the Yolo Bypass. Twelve cores collected in the Yolo Bypass were used to create a geochemical and mineralogical fingerprint of the bypass. Sediment in the bypass that contains HMS is distinguishable from the Coast Ranges sediment. The most distinguishable geochemical signatures of sediment from the Coast Ranges are that they have higher averages of Hg concentrations, Al/Ca, Ni/Zr, and Q/P values whereas sediment from the Sierra Nevada has higher averages of CaO and Fe_2O_3 percentages, Pb concentrations, and Ca/Sr values. The most distinguishable chemical and mineralogical signature of HMS is that HMS has higher Hg concentrations, Al/Ca values, and Q/P values, in addition to lower CaO percentages, Ca/Sr values, and Ni/Zr values compared to pre-mining sediment. The HMS has definite geochemical and mineralogical signatures; however, Hg concentrations throughout the bypass have minimal relationships to other geochemical and mineralogical indices and therefore Hg concentrations and chemical and mineralogical indices are independent of each other.

Each hydraulic band exhibits different geochemical and mineralogical signatures allowing for ease in differentiating between the bands. The Cache Creek band (T2) has the highest Al/Ca, Ni/Zr, and Hg concentrations. The Knights Landing Ridge Cut band (T3) Has the lowest Hg concentrations. The Sacramento River band (T4) has the highest Pb concentrations and Fe_2O_3 percentages. The Sacramento band (T4) has the lowest Q/P value

while the Putah Creek band (T1) has the highest Q/P value. These distinguishable signatures show how little lateral mixing occurs throughout the bypass.

The effects of gold and mercury mining can be seen in northern California, as large amounts of sediment were displaced and deposited elsewhere. The geochemical and mineralogical fingerprint of this sediment can benefit efforts to control and manage the mercury-contaminated sediment within the Yolo Bypass. Our knowledge of sedimentation in the bypass would be improved by applying dating techniques to the sediment samples. Studies like this are essential to better understand environments that contain HMS, as HMS carries many different contaminants.

REFERENCES CITED

Actlabs, 2018, Exploration Geochemistry: http://actlabs.com (accessed January 2018).

Allen, V.T., 1929, The Ione formation of California: University of California Publications in Geological Sciences Bulletin, v. 18, no. 14, p. 347-448.

Alpers, C.N., 2017, Arsenic and mercury contamination related to historical gold mining in the Sierra Nevada, California: Geochemistry: Exploration, Environment, Analysis, v. 17, no. 2, p. 92-100, doi:10.1144/geochem2016-018.

Alpers, C.N., Antweiler, R.C., Taylor, H.E., Dileanis, P.D., and Domagalski, J.L., 2000, Metals transport in the Sacramento River, California, 1996-1997: Volume 2: Interpretation of metal loads: U.S. Geological Survey Water-Resources Investigations Report 00-4002, 106 p., https://pubs.usgs.gov/wri/wrir00-4002/vol2.book.pdf.

Alpers, C.N., and Hunerlach, M.P., 2000, Mercury contamination from historic gold mining in California: U.S. Geological Survey Fact Sheet 061-00, 6 p., https://pubs.usgs.gov/fs/2000/fs06100/pdf/fs06100.pdf.

Averill, C.V., 1946, Placer mining for gold in California: California State Division of Mines and Geology Bulletin 135, 377 p.

Barnes, I., O'Neil, J.R., Rapp, J.B., and White, D.E., 1973, Silica-carbonate alteration of serpentine: Wall rock alteration in mercury deposits of the California Coast Ranges: Economic Geology, v. 68, p. 388-398, doi:10.2113/gsecongeo.68.3.388.

Barthold, K.F., Tyralla, C., Schneider, K., Vaché, K.B., Frede, H., and Breuer, L., 2011, How many tracers do we need for end member mixing analysis (EMMA)? A sensitivity analysis: Water Resources Research, v. 47, no. 8, p. 1-14, doi:10.1029/2011WR010604.

Barton, C.D., 2002, Clay minerals, *in* Lal, R., comp., ed., Encyclopedia of Soil Science: New York, Marcel Dekker, p. 187-192.

Bateman, P.C., 1992, Plutonism in the central part of the Sierra Nevada Batholith, California: U.S. Geological Survey Professional Paper 1483, 186 p., doi:10.3133/pp1483.

Blum, A.E., 1994, Feldspars in weathering, *in* Parsons, L., ed., Feldspars and Their Reactions, NATO ASI Series: Dordrecht, Springer, v. 421, p. 595-630, doi:10.1007/978-94-011-1106-5_15.

Bouse, R.M., Fuller, C.C., Luoma, S.N., Hornberger, M.I., Jaffe, B.E., and Smith, R.E., 2010, Mercury-contaminated hydraulic mining debris in San Francisco Bay: San Francisco Science Estuary and Watershed, v. 8, no. 1, p. 1-28, doi:10.15447/sfews.2010v8iss1art3.

Bradford, G.R., Change, A.C., Page, A.L., Bakhtar, D., Frampton, J.A., and Wright, H., 1996, Background Concentrations of Trace and Major Elements in California Soils: University of California, Division of Agriculture and Natural Resources, 32 p., https://ucanr.edu/sites/poultry/files/297094.pdf.

Bristow, T., 2018, Meeting discussing clay results by Stephanie Meursing. NASA Ames, November 9, 2018.

California Department of Fish and Game, 2008, Yolo Bypass Wildlife Area Land Management Plan: California Department of Fish and Game Yolo Bypass Wildlife Area, 367 p., https://cawaterlibrary.net/wp-content/uploads/2017/11/Yolo-Wildlife-Area-LMP-1.pdf.

Cassel, E.J., and Graham, S.A., 2011, Paleovalley morphology and fluvial system evolution of Eocene-Oligocene sediments ("auriferous gravels"), northern Sierra Nevada, California: Implications for climate, tectonics, and topography: Geological Society of America Bulletin, v. 123, p. 1699-1719.

Cassel, E.J., Graham, S.A., Chamberlain, C.P., and Henry, C.D., 2012, Early Cenozoic topography, morphology, and tectonics of the northern Sierra Nevada and western basin and range: Geosphere, v. 8, no. 2, p. 229-249, doi:10.1130/GES00671.1.

Chapin III, F.S., Matson, P.A., and Vitousek, P.M., 2011, Principles of Terrestrial Ecosystem Ecology, Second Edition: Geology, Soils, and Sediments: New York, Springer-Verlag, 529 p.

Cox, P.A., 1989, The Elements: Their Origin, Abundance, and Distribution: Oxford, England, Oxford University Press, 207 p.

Crain, D., and Lysy, C., 2016, Outlier Analysis: A Step-by-Step Guide, Version 1.0: Rockville, MD, Westat: IDEA Data Center, 20 p.

Doebelin, N., and Kleeberg, R., 2015, Profex: A graphical user interface for the Rietveld refinement program BGMN: Journal of Applied Crystallography, v. 48, p. 1573-1580, doi:10.1107/S1600576715014685.

Domagalski, J., 1998, Occurrence and transport of total mercury and methylmercury in the Sacramento River Basin, California: Journal of Geochemical Exploration, v. 64, p. 277-291, doi:10.1016/S0375-6742(98)00038-7.

Domagalski, J., 2001, Mercury and methylmercury in water and sediment of the Sacramento River Basin, California: Journal of Applied Geochemistry, v. 16, p. 1677-1691, doi:10.1016/S0883-2927(01)00068-3.

Domagalski, J.L., Slotten, D.G., Alpers, C.N., Suchanek, T.H., Churchill, R., Bloom, N., Ayers, S.M., and Clickenbeard, J., 2004, Summary and synthesis of mercury studies in Cache Creek watershed, California, 2000-01: U.S. Geological Survey Water-Resources investigations Report 03-4335, 30 p., https://pubs.usgs.gov/wri/wri034335/wri_034335.pdf.

Fitzpatrick R.W., and Chittleborough, D.J., 2002, Titanium and zirconium minerals, *in* Dixon J.B., ed., Soil Mineralogy with Environmental Applications: Madison, WI, Soil Science Society of America, v. 7, p. 667-690, doi:10.2136/sssabookser7.c22.

Gates-Rector, S.D., and Blanton, T.N., 2019, The powder diffraction file: A quality materials characterization database: Powder Diffraction, v. 34, no. 4, p. 352-360.

Gilbert, G.K., 1917, Hydraulic-mining debris in the Sierra Nevada: U.S. Geological Survey Numbered Series 105, 154 p., doi:10.3133/pp105.

Goldhaber, M.B., Morrison, J.M., Holloway, J.M., Wanty, R.B., Helsel, D.R., and Smith, D.B., 2009, A regional soil and sediment geochemical study in northern California: Applied Geochemistry, v. 24, no. 8, p. 1482-1499, doi:10.1016/j.apgeochem.2009.04.018.

Hunerlach, M.P., Rytuba, J.J., and Alpers, C.N., 1999, Mercury contamination from hydraulic placer-gold mining in the Dutch Flat mining district, California: U.S. Geological Survey Water-Resources Investigations Report 99-4018B, v. 2, p. 179-189.

Jackson, M.L., 1985, Soil Chemical Analysis – Advanced Course: Madison, WI, published by author, 2nd ed., 500 p.

James, L.A., 1989, Sustained storage and transport of hydraulic gold mining sediment in the Bear River, California: Annals of the American Association of Geographers, v. 79, no. 4, p. 570-592, http://www.jstor.org/stable/2563648.

James, L.A., 1991, Quartz concentration as an index of sediment mixing: Hydraulic mine-tailings in the Sierra Nevada, California: Geomorphology, v. 4, no. 2, p. 125-144, doi:10.1016/0169-555X(91)90024-5.

James, L.A., and Singer, M.B., 2008, Development of the lower Sacramento Valley flood-control system: Historical perspective: Natural Hazards Review, v. 9, no. 3, p. 125-135, doi:10.1061/(ASCE)1527-6988(2008)9:3(125).

James, L.A., Singer, M.B., Ghoshal, S., and Megison, M., 2009, Historical channel changes in the lower Yuba and Feather Rivers, California: Long-term effects of contrasting river-management strategies, *in* James, L.A., Rathburn, S.L., and Whittecar, G.R., eds., Management and Restoration of Fluvial Systems with Broad Historical Changes and Human Impacts: Geological Society of America Special Paper 451, p. 57–81, doi:10.1130/2008.2451(04).

Kabata-Pendias, A., 2001, Trace Elements in Soils and Plant: Boca Raton, CRC Press, 3rd ed., 403 p., doi:10.1201/9781420039900.

Kelley, R.L., 1989, Battling the Inland Sea: Berkeley, University of California Press, 395 p.

Kelly, E.G., Subasinghe, G.K.N.S., and Walsh, D.E., 1995, The sluice box-an evaluation: Minerals Engineering, v. 8, no. 11, p 1397-1425, doi:10.1016/0892-6875(95)00105-Y.

Kongchum, M., Hudall, W.H., and Deluane, R.D., 2011, Relationship between sediment clay minerals and total mercury: Journal of Environmental Science and Health, Part A, Toxic Hazardous Substances and Environmental Engineering, v. 46, no. 5, p. 534-539, doi:10.1080/10934529.2011.551745.

Lindgren, W., 1911, The Tertiary gravels of the Sierra Nevada of California: U.S. Geological Survey Professional Paper 73, 226 p., doi:10.3133/pp73.

Lucas, J., El Faleh, E.M., and Prevot, L., 1990, Experimental study of the substitution of Ca by Sr and Ba in synthetic apatites, *in* Trappe, J., ed., Phanerozoic Phosphorite Depositional Systems, A Dynamic Model for a Sedimentary Resource System: London, Geological Society, Special Publication, v. 52, p. 33-47.

Marvin-DiPasquale, M., Windham-Myers. L., Agee, J.L., Evangelos, K., Kieu, L.H., Fleck, J.A., Alpers, C.N., and Stricker, C.A., 2013, Methylmercury production in sediment from agricultural and non-agricultural wetlands in the Yolo Bypass, California, USA: Science of the Total Environment, v. 484, p. 288- 299, doi:10.1016/j.scitotenv.2013.09.098.

McLean, J., and Bledsoe, B., 1992, Behavior of metals in soils: Washington, D.C., United States Environmental Protection Agency EPA/540/S-92/018, 25 p.

Mix, H. T., Ibarra, D. E., Mulch, A., Graham, S. A., and Chamberlain, C. P., 2015, A hot and high Eocene Sierra Nevada: Geological Society of America Bulletin, v. 128, no. 3-4, p. 531-542, doi:10.1130/B31294.1.

Moore, D.M., and Reynolds Jr., R.C., 1989, X-ray Diffraction and the Identification and Analysis of Clay Minerals: New York, Oxford University Press, 332 p.

Morrison, J.M., Goldhaber, M.B., Lee, L., Holloway, J.M., Wanty, R.B., Wolf, R.F., and Ranville, J.F., 2009, A regional-scale study of chromium and nickel in soils of northern California, USA: Applied Geochemistry, v. 24, no. 8, p. 1500-1511, doi:10.1016/j.apgeochem.2009.04.027.

Morrison, J.M., Goldhaber, M.B., Mills, C.T., Breit, G.N., Hooper, R. L., Holloway, J.M., Diehl, S.F., and Ranville, J.F., 2015, Weathering and transport of chromium and nickel from serpentinite in the Coast Range ophiolite to Sacramento Valley, California, USA: Applied Geochemistry, v. 62, p. 72-86, doi:10.1016/j.apgeochem.2015.05.018.

Mykytyn, T., 2021, Distribution of Hg-laden sediment in the Yolo Bypass, California [Master's thesis]: San Jose State University.

Nakamura, T.K., Singer, M.B., and Gabet, E.J., 2018, Remains of the 19th Century: Deep storage of contaminated hydraulic mining sediment along the lower Yuba River, California: Elementa: Science of the Anthropocene, v. 16, no. 70, p. 1-17, doi:10.1525/elementa.333.

Nesbitt, H.W., and Young, G., 1982, Early Proterozoic climates and plate motions inferred from major element chemistry and lutites: Nature, v. 299, p. 715-717, doi:10.1038/299715a0.

Office of Emergency Services, 2018, 2018 Yolo operational area multi-jurisdictional hazard mitigation plan: County of Yolo, 330 p.

Oze, C., Fendorf, S., Bird, D.K., and Coleman, R.G., 2004, Chromium geochemistry in serpentinized ultramafic rocks and serpentine soils from the Franciscan complex of California: American Journal of Science, v. 304, p. 67-101, doi:10.2475/ajs.304.1.67.

Petersen, M.D., 1983, The use of the "immobile" elements Zr and Ti in lithogeochemical exploration for massive sulphide deposits in the precambrian pecos greenstone belt of northern New Mexico: Journal of Geochemical Exploration, v. 19, no. 1-3, p. 615-617, doi:10.1016/0375-6742(83)90051-1.

Pett-Ridge, J.C., Derry, L.A., and Barrows, J.K., 2009, Ca/Sr and 87Sr/86Sr ratios as tracers of Ca and Sr cycling in the Rio Icacos watershed, Luquillo Mountains, Puerto Rico: Chemical Geology, v. 267, no. 1-2, p. 32-45, doi:10.1016/j.chemgeo.2008.11.022.

Poppe, L.J., Paskevich, V.F., Hathaway, J.C., and Blackwood, D.S., 2001, A laboratory manual for X-ray powder diffraction: U.S. Geological Survey Open-File Report 01-041, 89 p., doi:10.3133/ofr0141.

Probst, A., Gh'mari, A., Aubert, D., Fritz, B., and McNutt, R., 2000, Strontium as a tracer of weathering processes in a silicate catchment polluted by acid atmospheric inputs Strengbach, France: Chemical Geology, v. 170, no. 1-4, p. 203-219, doi:10.1016/S0009-2541(99)00248-X.

Schemel, L.E., Cox, M.H., Hager, S.W., and Sommer, T.R., 2002, Hydrology and chemistry of floodwaters in the Yolo Bypass, Sacramento River system, California, during 2000: U.S. Geological Survey Water Resources Investigations Report 02-4202, 65 p., https://pubs.usgs.gov/wri/wri02-4202/WRI02-4202.pdf.

Shelton, L.R., and Capel, P.D., 1994, Guidelines for collecting and processing samples of stream bed sediment for analysis of trace elements and organic contaminants for the national water-quality assessment program: U.S. Geological Survey Open File Report 94-458, 20 p., https://pubs.usgs.gov/of/1994/0458/report.pdf.

Singer, M.B., Aalto, R., and James, L.A., 2008, Status of the lower Sacramento Valley flood-control system within the context of its natural geomorphic setting: Natural Hazards Review, v. 9, no. 3, p. 104-115, doi:10.1061/(ASCE)1527-6988(2008)9:3(104).

Solt, M.J., Deocampo, D.M., and Norris, M., 2015, Spatial distribution of lead in Sacramento, California, USA: International Journal of Environmental Research and Public Health, v. 1, no. 3, p. 3174-3187, doi:10.3390%2Fijerph120303174.

Sommer, R.S., Harrell, W.C., and Swift, J.S., 2008, Extreme hydrologic banding in a large-river floodplain, California, USA: Hydrobiologia, v. 598, p. 409-415, doi:10.1007/s10750-007-9159-1.

Sommer, T., Harrell, B., Nobriga, M., Brown, R., Moyle, P., Kimmerer, W., and Schemel, L., 2001, California's Yolo Bypass: Evidence that flood control can be compatible with fisheries, wetlands, wildlife, and agriculture: Fisheries, v. 26, no. 8, p. 6-16, doi:10.1577/1548-8446(2001)026<0006:CYB>2.0.CO;2.

Springborn, M., Singer, M.B., and Dunne, T., 2011, Sediment-adsorbed total mercury flux through Yolo Bypass, the primary floodway and wetland in the Sacramento Valley, California: Science of the Total Environment, v. 412-413, p. 203-213, doi:10.1016/j.scitotenv.2011.10.004.

Studemeister, P.A., 1984, Mercury deposits of western California: aAn overview: Mineral Deposita, v. 19, p. 202-207, doi:10.1007/BF00199786.

Thrush, P.W., 1968, A Dictionary of Mining, Mineral, and Related Terms: Washington, D.C., U.S. Department of the Interior, Bureau of Mines, U.S. Government Printing Office, 1269 p.

Tipp, C.M., and Gabet, E.J., 2020, Reconstruction of the original extent of the Tertiary pre-volcanic gravels in the northern Sierra Nevada (CA): Implications for the range's paleotopography: American Journal of Science, v. 320, p. 815-850, doi:10.2475/12.2020.01.

Turner, H.W., 1899, The granitic rocks of the Sierra Nevada: The Journal of Geology, v.7, no. 2, p. 141-162, doi:10.1086/608320.

US Army Corps of Engineers, 2003, Lower Cache Creek, Yolo County, CA City of Woodland and Vicinity: Sacramento District, 277 p.

Valkovic, V., 1983, Sample preparation techniques in trace element analysis by x-ray emission spectroscopy: International Atomic Energy Agency Technical Document 300, 188 p.

Wei, G., Li, X.-H., Liu, Y., and Liang, X., 2006, Geochemical record of chemical weathering and monsoon climate change since the early Miocene in the South China Sea: Paleoclimatology, v. 21, no. 4, p. 1-11, doi:0.1029/2006PA001300.

Wiener, J.G., Bodaly, R.A., Brown, S.S., Lucotte M.C., Porcella, D.B., Reash, R.J., and Swain, E.B., 2007, Monitoring and evaluating trends in methylmercury accumulation in aquatic biota, *in* Harris, R., Krabbenhoft, D.P., Mason, R., Murray, M.W., Reash, R.J., and Saltman, T., eds., Ecosystem Responses to Mercury Contamination: Indicators of Change: New York, CRC Press, p. 87-122, doi:10.1201/9780849388897.ch4.

Wright, S.A. and Schoellhamer, D.H., 2004, Trends in the sediment yield of the Sacramento River, California, 1957-2001: San Francisco Estuary and Watershed Science, v. 2, no. 2, p. 1-14, doi:10.15447/sfews.2004v2iss2art2.

Yang, J.H., and Du, Y.S., 2017, Weathering geochemistry and paleoclimate implications of the Early Permian mudstones from eastern Henan Province, North China: Journal of Paleogeography, v.6, no. 4, p. 370-380, doi:10.1016/j.jop.2017.08.003.

Yeend, W. E., 1974, Gold-bearing gravel of the ancestral Yuba River, Sierra Nevada, California: United States Geological Survey Professional Paper 772, 50 p., doi:10.3133/pp772.

Yu, T., Zhang, Y., and Zhang, Y., 2012, Distribution and bioavailability of heavy metals in different particle-size fractions of sediments in Taihu Lake, China: Chemical Speciation and Bioavailability, v. 24, no. 4, p. 201-215, doi:10.3184/095422912X13488240379124.

APPENDIX 1. SAMPLING SITES

(Modified from Thomas Mykytyn's Master's Thesis Proposal)

Entities responsible for parcels on selected sampling sites:

1. SACRAMENTO/SAN JOAQUIN DRAINAGE DISTRICT & DEPT. OF WATER RESOURCES

2. SACRAMENTO/SAN JOAQUIN DRAINAGE DISTRICT & DEPT. OF WATER RESOURCES

3. CONAWAY PRESERVATION GROUP LLC & 401 WATT AVE. STE

4. CONAWAY PRESERVATION GROUP LLC & 401 WATT AVE. STE

5. (VARIOUS SMALL PARCELS) EX: SWANSTON PROPERTIES ETAL & C/O MARTY SWANSTON

6. CALIFORNIA STATE OF & C/O DEPT OF FISH & GAME

7. CALIFORNIA STATE OF & DEPT OF FISH & GAME

8. CALIFORNIA STATE OF & DEPT OF FISH & GAME

9. FROST JAMES R & P.O. BOX 37

10. PFC INC & P.O. BOX 5058

11. WESTLANDS WATER DISTRICT & ATTN DAVE CIAPPONI

12. WESTLANDS WATER DISTRICT & ATTN DAVE CIAPPONI

Sites are numbered from west to east and north to south (site 1 is the northernmost, site 12 is the southeasternmost; see Figure 1).

APPENDIX 2. DEPTH PROFILE GRAPHS OF BOREHOLE CORES IN THE YOLO BYPASS